THREE-STAGE FORMATION OF GREENSTONE-HOSTED OROGENIC GOLD DEPOSITS IN THE VAL-D'OR MINING DISTRICT, ABITIBI, CANADA: EVIDENCE FROM PYRITE AND TOURMALINE

Lucille M. Daver[1,*], Michel Jebrak[1], Georges Beaudoin[2], Robert B. Trumbull[3]

1 – Département des sciences de la Terre et de l'atmosphère, Université du Québec à Montréal, QC, Canada

2 – Département de géologie et de génie géologique, Université Laval, Québec, QC, Canada

3 –German Research Centre for Geosciences GFZ, Telegrafenberg, 14473 Potsdam, Germany

* to whom the correspondence should be addressed: daver.lucille@uqam.ca

Keywords Orogenic gold, tourmaline, pyrite, LA-ICP-MS, element mapping, boron isotopes, Val-d'Or, Abitibi

Declarations of interest: none

ABSTRACT

Orogenic gold deposits are the most widespread type of gold deposit worldwide, defining important exploration targets in Precambrian greenstone belts. Here, we refine the model for orogenic gold formation in the world-class Val-d'Or mining district (Quebec, Canada) using geochemical, isotopic and mineralogical data from quartz-tourmaline-carbonate (QTC) veins from several deposits across the district. Multi-element (Ag, As, Au, B, Ba, Co, Mg, Mo, Ni, and Pb) pyrite mapping, as well as major, trace, and rare earth element variations in tourmaline, define a three-stage paragenesis across several deposits. The first, reduced phase crystallized the quartz-carbonate-gold association in the veins; the second, oxidized phase favored tourmaline and barite crystallization (barite was not previously reported from this district); the third phase involved a reduced fluid and the crystallization of non-auriferous, As-Co-Ni-rich cubic pyrite, and tourmaline. Boron isotope ratios of tourmaline vary from -15.6 to -7.7 ‰, which is attributed to the mixing of at least two fluids, one related to a deep, metamorphic source and the other to shallower, possibly relict formation water. A systematic regional pattern in B-isotope variation is found, with lighter values in the volcanic rocks and heavier ones in or close to intrusions, which suggests different mixing proportions in the vein field from NE to SW.

1. Introduction

Archean greenstone belts host most of the world's high-grade orogenic gold deposits. Among them, the Abitibi subprovince in the southeastern part of the Precambrian Canadian Shield hosts hundreds of gold deposits, distributed over more than 200 km along two major connected reverse shear zones: the Cadillac-Larder Lake Fault Zone (CLLFZ) to the south and the Porcupine-Destor Fault Zone (PDFZ) to the north (Fig. 1; Robert, 1994). The Val-d'Or mining district is located in the eastern part of the Abitibi subprovince along the CLLFZ. It hosts approximately 55 auriferous quartz-tourmaline-carbonate (QTC) vein deposits spread over a 40 by 15 km area (Fig. 1), which together contain a total of ~20 million ounces Au (Rafini, 2014). In this district, the Sigma QTC auriferous veins have become one of the archetypes of orogenic gold deposits (Sibson *et al.*, 1988; Robert, 1994; Gaboury, 1999; Neumayr and Hagemann, 2002).

Based on structural and hydrothermal characteristics (mineral assemblages and alteration), the Abitibi gold-bearing QTC vein field is commonly understood to represent a single hydrothermal event (Robert, 1994). Mineralization is suggested to have occurred at the end of the formation of the Superior Province (~2.6 Ga), or shortly thereafter, through the process of seismic pumping, whereby fluid transport occurred in seismically-induced pulses (Sibson *et al.*, 1975; Boullier and Robert, 1992). This process resulted in the circulation of mineralized hydrothermal fluids into third-order fault systems of the CLLFZ during earthquake rupturing episodes. However, the precise chronology of this episodic infilling is still debated (Kerrich and Ludden, 2000; Robert *et al.*, 2005).

Previous isotopic studies in the Val-d'Or district (Beaudoin and Pitre, 2005; Beaudoin and Chiaradia, 2016) suggest a fluid mixing scenario for the mineralizing fluid two different fluid reservoirs where the H-O-Sr isotope values of the vein assemblage are interpreted to reflect two end-member fluids: one metamorphic and another supracrustal (Beaudoin and

Chiaradia, 2016). A preliminarily tourmaline B-isotope study by Beaudoin *et al.*, (2013) suggested the presence of a regional southwest to northeast isotopic zonation in the district.

The objective of this study is to improve the understanding of the temporal and genetic relationships of QTC vein mineralogical assemblages in the Val-d'Or district through a detailed investigation of pyrite and tourmaline. The current formation model proposes multiple fluid pulses during a single hydrothermal event involving the mixing of metamorphic and upper crustal fluids (Robert, 1994; Gaboury, 1999; Neumayer and Hagemann, 2002; Beaudoin and Chiaradia, 2016). To better define this model, samples from several deposits distributed across the region were selected to obtain a regional coverage that is representative of the geochemical variability in the vein field (Fig. 1). Pyrite and tourmaline were chosen as the minerals best suited to investigate the paragenetic evolution of the system. Gold in the Val-d'Or district is mainly associated with pyrite, either as inclusions and/or in the pyrite lattice. Pyrite formed episodically during QTC vein formation, and its chemical variability reflects changes in hydrothermal fluid chemistry and in mineralizing conditions (P, T, redox) throughout its mineralization history (Large *et al.*, 2009; Goldfarb and Groves, 2015). Tourmaline has a broad stability range and a wide chemical variability, which responds to changes in fluid composition (Van Hinsberg and Schumacher, 2009; Henry *et al.,* 2011; Dutrow and Henry, 2011). Furthermore, B-isotope variations in tourmaline can effectively fingerprint fluid sources and identify regions where fluid mixing has occurred (Krienitz *et al.,* 2008 ; Zhang *et al.*, 2014; Lambert-Smith *et al.,* 2016).

2. Geological setting

2.1 Val-d'Or mining district

The Val-d'Or QTC vein field is located at the tectonic boundary between the Abitibi volcanic subprovince and the Pontiac sedimentary subprovince of the Archean Superior

Province (Card and Ciesielki, 1986). The 200 km-long Cadillac-Larder Lake fault is a major shear zone (CLLFZ), which separates these two subprovinces (Fig.1). It represents a first-order fault, which dips steeply to the north and flattens at approximately 10 km depth (Green *et al.*, 1990; Robert, 1994). Second-order structures consist of 1 to 10 km-long and 1 to 100 m-wide faults with an E-W subvertical strike-slip in the Val-d'Or district (Robert, 1990). The third-order faults are smaller and more numerous, ranging from 1 m to 1 km in length, with strike-slip movement, and trending between NW and NE, dipping 35° to 75° to the south or north (Robert, 1990).

The Val-d'Or mining district is composed of ultramafic to intermediate volcanic rocks emplaced between 2714 Ma and 2702 Ma ± 2 Ma (Pilote *et al.* 1998; Scott *et al.* 2002). A series of syn-to-late tectonic intrusions dated from 2694 to 2680 Ma, including the Lamaque diorite at 2685 Ma (Jemielita, 1990) and the Bourlamaque pluton at 2699 ±1 Ma (Hanes *et al.,* 1992; Wong *et al.*, 1991; Jemielita *et al.*, 1990) crosscut the volcanic and intrusive rocks. Regional greenschist facies metamorphism occurred from 2693 to 2677 Ma (Hanes *et al.,* 1992; Feng and Kerrich, 1992) and was accompanied by regional shortening, forming a series of dominant E-W subvertical to moderately-dipping shear zones that host the QTC veins (Robert, 1990). Regional deformation ended with the convergence of the Abitibi and the Pontiac terranes along the CLLFZ at ~2670 Ma (Feng *et al.*, 1992).

The district hosts two overlapping auriferous vein types: early quartz-carbonate veins and later quartz-tourmaline-carbonate (QTC) veins. The early quartz-carbonate auriferous vein field formed before regional metamorphism (>2690 Ma). These veins are folded and boudinaged within sub-vertical shear zones, and crosscut by regional mafic dykes (Robert, 1990). The later, QTC-type veins are the subject of this study. They were emplaced after metamorphism (<2670 Ma) and are crosscut on a regional scale by Archean intrusions and mafic dykes, but not by Proterozoic dykes (Latulippe, 1966; Robert, 1994; Couture *et al.*, 1994).

The QTC veins were emplaced in sub-vertical reverse shear zones as fault-filled lenses, or near the shear zones in sub-horizontal extensional veins (Robert *et al*., 1995).

These two vein fields are interpreted as having formed in two successive hydrothermal events (Robert, 1994; Robert and Brown, 1986; Couture, 1994), which likely shared the same fluid conduit: the first-order fault system (Robert, 1990; Neumayr and Hagemann, 2002; Beaudoin and Pitre, 2005). However, the QTC vein field is better endowed with mineralization, and hosts several economic deposits with similar mineralogical characteristics (Robert and Brown, 1986; Fig.1). Robert (1994) suggested that the fault system worked as an interconnected system to allow for fluid circulation.

2.2. Sample descriptions

Six QTC veins were sampled from four mines (red symbols in Fig. 1): one from the Goldex mine, three from the Lamaque mine (two from the Triangle and one from the Parallel zones), one from the Lac Herbin mine (production ended in 2016), and one from the Beaufor mine (production ended in 2019). The sampled mines are aligned along with a SW-NE trend across the Val-d'Or mining district (Fig. 1). They occur in two different host lithologies: (1) local diorite intrusions in volcanic rocks (Goldex and Lamaque QTC veins), and (2) the dioritic Bourlamaque pluton (Lac Herbin and Beaufor QTC veins). The Lamaque samples were selected from two different exploration zones, 2 km apart: the Triangle zone (Lamaque-T) and the Parallel zone (Lamaque-P).

2.2.1 Goldex

The Goldex mine is located 1.5 km north of the CLLFZ, in the southern part of the district. QTC veins and veinlets occur inside a 0.1-0.25 km by 3.8 km quartz-diorite intrusion in the metabasalts of the Jacola Formation (Genest, 2012). The mineralization was emplaced as centimeter-to-decimeter veins and veinlets in a complex stockwork system. Veins present

proximal (±0.5 m thick) albite and sericite-rich alteration haloes and a biotite-chlorite distal alteration halo 3-10 m thick (Genest, 2012). Sample 91 is from a quartz vein with disseminated tourmaline and pyrite in contact with a feldspathic and chlorite alteration. The sample was collected from a drill core in a stockwork vein system at 134 m depth (Fig.2A).

2.2.2. Lamaque

The Triangle and Parallel zones are part of the Lamaque deposit, located in the southern part of the Val d'Or district. The well-know Sigma mine nearby represents the northern extension of the Lamaque deposit (Robert and Brown, 1986). Together, they produced over ten million oz of gold. The Triangle zone is located 2.5 km from the historical Lamaque mine. It has been an operational mine since March 2019 (Eldorado gold), with an average grade of 7 g/t Au (Beauregard et al., 2014). The Parallel zone is a current exploration project located 500 m from the Lamaque deposit and 2 km from the Triangle zone. QTC veins with disseminated pyrite occur in an 800 x 400 m dioritic intrusion in the andesite of the Val-d'Or Formation (Poulsen *et al.*, 2000). Veins were emplaced in a series of sub-vertical shear zones and fractures, and also as extensional shear vein splays (Beauregard et al., 2014). Sample 85 is from a quartz-tourmaline vein with pyrite and chlorite. Sample 87 is from a quartz-tourmaline vein with pyrite and a larger proportion of chlorite and some K-feldspar veining. Samples 85 and 87 were collected from the same drill core in the Triangle zone, at 208.5 m and 211.5 m depths respectively (Fig. 2B and Fig. 2C). Sample 87 presents pervasive chlorite and a K-feldspar veinlets. Sample 88 represents quartz-tourmaline veins with disseminated pyrite, collected from the Parallel zonein a drill core at 212 m depth (Fig. 2D).

2.2.3. Lac Herbin

The Lac Herbin mine is located in the center of the 170 km^2 Bourlamaque pluton, which is dioritic to tonalitic in composition (Lemarchand, 2012). QTC veins emplaced in shear zones from less than 1 to 3.5 m width (Rezeau et al., 2017). Several deformed dioritic dykes crosscut

the deposit parallel to the QTC veins. Sample 73 is a centimeter-wide quartz vein with a veinlet of sulfides and tourmaline veinlets. Parallel veinlets of tourmaline and pyrite-chalcopyrite are separated within the quartz vein (Fig. 2E). The sample was collected in the underground part of the mine, from an E-W trending shear zone at level 15.

2.2.4 Beaufor

The Beaufor mine is located in the eastern part of the Bourlamaque pluton. Quartz-tourmaline veins, with pyrite, chalcopyrite, and chlorite were emplaced in decimeter-to-meter lenses within subhorizontal tensional shears zones. The Beaufor deposit formed at the border of the Bourlamaque pluton and mafic rocks of the Dubuisson Formation. Sample 11 is from a quartz-tourmaline vein with pyrite, chalcopyrite, and chlorite, and was collected from a 2 m-wide crack-and-seal vein in the 22C-355 level of the underground mine (Fig. 2F).

3. Materials and methods

The three veins from Lamaque were samples from drill cores, and those from Goldex, Lac Herbin and Beaufor were hand samples. All were sampled inside the representative quartz vein and contain visible sulfides and tourmaline. Samples were crushed and sulfide minerals were separated by density from the lighter silicates using a hydroseparator. The heavy mineral assemblage, including gold and its alloys (Ag, Te) was characterized via SEM-EDX (Fig. 3) on isolated grains with a Hitachi S-3400N type II (4 detectors) at 15 kV.

Representative tourmaline grains, ranging from 60 to 600 μm long, were handpicked from each sample under a binocular microscope and set in two epoxy mounts. Major, trace, and rare earth elements were measured on one sample mount, which contained 48 tourmaline grains - eight per sample. They were analyzed using a New wave 213 nm Nd-YAG laser ablation system coupled with an iCAP Qc ICP-MS at McGill University, Montréal, Canada. The 60 μm beam made a 10 μm deep ablation channel along the length of each tourmaline grain (between 70 and

300 μm) at 6 μm/s. The laser is operated continuously at 10 Hz and 65% energy. The energy of the laser is 0.244 mJ, with a flux of 8.63 J/cm2. The washing time of the laser is 40 s and heating time is 30 s. The instrumental mass fractionation and analytical quality were determined by repeat analysis of reference materials, NIST 160, NIST 612, and NIST 614.

Boron isotopes were measured on 76 representative tourmaline grains from the six samples, which were mounted in the second epoxy mount. The analysis was undertaken using the CAMECA 1280-HR secondary ion mass spectrometer (SIMS) at the German Research Centre for Geosciences (GFZ) in Potsdam, Germany (Table 2). The sample mount was cleaned and coated with high-purity gold before SIMS analyses. The instrument was tuned with a $^{16}O^-$ ion beam of ca. 3 nA intensity, focused to a 5 μm spot on the sample surface. Secondary ions were measured in multi-collector mode using Faraday cups. For further analytical details of the tourmaline analysis carried out at GFZ using the 1280-HR instrument, see Lambert-Smith *et al.* (2016). The instrumental mass fractionation and analytical quality were determined by repeat analysis of tourmaline reference materials, Harvard 112566 schorl and Harvard 108796 dravite, which span the compositional range of the tourmalines studied here. Each analysis consisted of 20 measurements at the ^{10}B and ^{11}B mass stations, and the internal precision was typically 0.1 ‰ (1 s.d.). The repeatability determined from multiple analyses of the reference tourmalines during the analytic session was better than 0.3 ‰ individually (1 sd, n = 54). The overall repeatability calculated for both reference tourmalines together was 0.6 ‰ (1 sd), which includes any chemical matrix effect in the shorl-dravite composition range. Boron isotope ratios are reported in delta notation ($\delta^{11}B = (^{11}B/^{10}B)_{sample}/(^{11}B/^{10}B)_{std}$) in per mil (‰) relative to the NIST SRM 951 standard (Catanzaro *et al.*, 1970).

Pyrite grains in thin-section were measured by laser-ablation ICPMS in element-mapping mode or Ag, As, Au, B, Ba, Co, Mg, Mo, Ni, and Pb. Five pyrite grains were mapped using a Resonetics S-155-LR with a 193 nm Excimer laser ablation system coupled to an Agilent 7700x

quadrupole ICP-MS at the University of New Brunswick, Fredericton, Canada. The instrumental mass fractionation and analytical quality were determined by repeat analysis of reference materials NIST 610 and MASS1. Eight-to-10 µm-deep ablations were perform at a travel speed of 25 µm/s with a 36 µm-diameter beam. The analyzed pyrites grains were selected based on their size (>5 mm) and the presence of visible zonation in reflected light observations. The selected grains represent the dominant grain morphology in the QTC veins from the Lac Herbin and Goldex deposits, as compared to less abundant, smaller, more idiomorphic cubic grains, which are late-stage and have no gold inclusions. Pyrites with a central pitted texture and smooth halo were found in thin-sections of the six samples and were analyzed.

4. Results

4.1. Mineralogy

The QTC veins contain a similar mineral assemblage in all of the samples, comprising quartz, carbonate, tourmaline, pyrite, K-feldspar, muscovite, chlorite ± pyrrhotite, chalcopyrite, molybdenite, and scheelite (Table 1; Fig. 2). Pyrite is disseminated in the veins and ranges from a micrometer in size, and up to 1 centimeter wide in the samples. It can represent up to 10% of the vein mineral assemblage, either aggregated or more sporadic. Pyrite is the most abundant sulfide and is gold-bearing (Fig. 3 and 4), except for a later generation of smaller, idiomorphic cubic grains, which are barren. SEM-EDX measurements on pyrite indicate the presence of micro-inclusions of native gold or electrum. At the Lamaque deposit (the Triangle and Parallel deposits are described together), gold is frequently associated with tellurides, including calaverite ($AuTe_2$) and krennerite (Au_3AgTe_3). The Lac Herbin and Beaufor deposits also contain euhedral, Ni-Co-rich arsenopyrites.

Tourmaline occurs disseminated or in late veinlets within the QTC veins, and both were sampled for the study (Fig. 2). These tourmaline veinlets contain disseminated cubic pyrites with few gold inclusions on their surface caused by a late remobilzation. Despite the overall

similarity in the mineralogy of the vein material from one deposit to another, there are slight differences in mineral proportions (Table 1). This variation is linked to a change from quartz to albite and microcline in the vein, particularly for quartz and carbonate, which represent ~50% of Goldex and Lamaque vein modal mineralogy and ~90% of Lac Herbin and Beaufor vein modal mineralogy. For all deposits sampled, tourmaline represents ~2% of the sample material. In some veins, tourmaline proportion can reach >50% of the vein assemblage.

4.2. Element mapping in pyrite

Element mapping of pyrite in thin sections from the Lac Herbin and Goldex deposits gave consistent results regarding the pyrite paragenesis (Fig. 4 and 5). Mapping of Ag, As, Au, B, Ba, Co, Mg, Mo, Ni, and Pb enables different pyrite stages to be distinguished. Three observable geochemically distinct zones in the grains suggest three generations of pyrite growth (Fig. 4 and 5). The first generation of pyrite is in the crystal cores (Fig 4A and 5A), with a ragged border (Pyrite 1). It contains numerous 10-30 µm inclusions, including gold and relatively Mg-rich phase too small for identification. The ragged border of Pyrite 1 indicates dissolution. The outer halo of this pyrite contains 250-200 µm diameter inclusions of B- and Ba-rich minerals, mainly tourmaline and barite (Fig. 4B and 5B). Pyrite 2 occurs as an overgrowth on Pyrite 1 and has a Co-rich composition (Fig. 4C and 5C). The composition of Pyrite 3 changes outward to an As- and Ni-rich composition with no further more association with gold (Fig. 4C and 5C). Pyrites 2 and 3 are inclusion-free. Where the grains showed late brittle deformation, gold and other metals (Ag, Mo, Pb) from pyrite cores (as inclusions or in the lattice) were remobilized into fractures and pores (Fig. 4D).

4.3. Major, trace and REE elements in tourmaline

The presence of tourmaline inclusions in Pyrite 1 suggests that tourmaline began to crystallize at the end of the Pyrite 1 formation. Tourmaline compositions on a district scale vary

from a Mg-rich to an Fe-rich composition, as indicated by the Fe/Mg and Na/Ca plots (Fig. 6A). The northeastern deposits (Beaufor and Lac Herbin) are dravitic (Mg-rich) and the southwestern deposits (Goldex and Lamaque) are schorlitic (Fe-rich) tourmalines. However, tourmaline trace element contents show no systematic trends. The average primitive mantle-normalized trace element values (McDonough and Sun, 1995) are heterogeneous among the deposits (Fig. 6B; Table A1). Most show Pb and Sr enrichment and Ce depletion compared with neighboring trace-elements (Fig. 6B). In general, tourmaline from the Lamaque deposit has higher trace-element concentrations than those from the other deposits, especially for U, Nb, Pb, Zr, for the REE generally, and for the HREE in particular (Fig. 6B). Tourmaline in all of the deposits shows a positive Eu anomaly, but this is less marked in the Lamaque tourmaline than for the other deposits.

4.4. Boron isotopes in tourmaline

Boron isotope analysis resulted in $\delta^{11}B$ values ranging from -15.6 to -7.7 ‰ (Fig 6C). Ten grains were typically analyzed from each deposit and the internal variations was found to be about 2-3 ‰ (Table 2). The B-isotope ratios from individual locations across the Val-d'Or district show a spatial pattern; the southwestern Goldex and Lamaque samples have lighter $\delta^{11}B$ values, from -15.6 to -9.1 ‰ whereas the Beaufor and Lac Herbin samples from farther east in the district yielded higher $\delta^{11}B$ values, from –11.2 to -7.7 ‰ (Fig. 7, Table 2). This apparently systematic increase in $\delta^{11}B$ values from west to east agrees with the results of an earlier study by Beaudoin *et al.,* 2013.

5. Discussion

Two interpretations are possible for the proposed three-phase evolution of the Val-d'Or mineralization based on the pyrite paragenesis: (1) multiple fluid pulses during a single hydrothermal event (Robert, 1994), or (2) multiple, discontinuous hydrothermal episodes

spread over a longer time span (Fontaine *et al.*, 2017; Molnár *et al.*, 2018). The similar mineralogical signature of the veins suggests a common origin for the vein forming fluid. The pyrite element mapping helps to distinguish between evolution during one continuous hydrothermal event versus an episodic mineralization scenario. The first would be recorded in the pyrite as continuous crystallization (Murowchick *et al.*, 1987; Román *et al.,* 2019), as is the case for the gradual variation between Pyrite 2 and Pyrite 3 (Fig. 4C and 5C). In contrast, the discontinuous growth and partial resorption between Pyrite 1 and Pyrite 2, suggests two distinct episodes in the vein field construction. This may be associated with episodic pulses of fluid rising through the CLLFZ fault system.

5.1. Phase 1

Phase 1 represents the beginning of vein formation with the first hydrothermal pulse. It crystallized the quartz-carbonate vein material and disseminated gold-bearing pyrite. The irregular shape of Pyrite 1, associated with abundant mineral inclusions and clustered pores, suggests fast crystallization and supersaturation conditions (Murowchick and Barnes, 1987; Wang *et al.*, 2012; Román et al., 2019). The Au maps and SEM-EDX analysis indicate an uneven gold distribution between the samples which corroborates the uneven gold content distribution in the district (Robert *et al.*, 2005). The gold content in the Sigma-Lamaque deposit is higher than that in the surrounding deposits in the Val-d'Or district (Robert *et al.*, 2005). In veins from the Lamaque deposit, gold is found as an alloy with Ag, Pb, and Te. In the other studied deposits, gold is either native or is associated with silver (Table 1). This difference could be caused by a Te-Ag-Pb-rich fluid that was restricted at the scale of Sigma-Lamaque deposit, and therefore only impacted this deposit.

5.2. Phase 2

Phase 2 began with the crystallization of tourmaline and barite at the end of Pyrite 1. The occurrence of barite in the veins and the positive Eu anomaly recorded in the tourmalines

indicate an oxidized fluid as tourmaline-barite forming-fluid. The dissolution border of Pyrite 1 indicates a reaction with this tourmaline-barite forming-fluid. Barite is less abundant than tourmaline in the deposits, and was only observed as inclusions in Pyrite 1.

5.3. *Phase 3*

Phase 3 started with a new pulse of hydrothermal fluids, which enabled a return to reduced conditions and the precipitation of more pyrite. Pyrite 2 and 3 are not auriferous. Pyrite 2 is Co-rich and Pyrite 3 is As-Ni-rich compared with Pyrite 1 (Fig. 4C and 5C). The homogenous distribution of Co, As and Ni in Pyrites 2 and 3 indicates that the Co, As, and Ni is structurally bound with the pyrite. Pyrite 2 and 3 show Co-rich and As-Ni-rich zonation patterns respectively, and are inclusion-free. Arsenic, nickel, and cobalt were introduced either during or after the oxidized phase (Phase 2), with the Phase 3 hydrothermal fluid pulse. Ni-Co-rich arsenopyrite also formed during phase 3. The pyrite zonation pattern suggests slow crystallization kinetics, under low-boiling (gradual cooling and physico-chemical variation) or non-boiling conditions in a less-sulfide-saturated environment (Murowchick and Barnes, 1987; Román *et al.*, 2019) compared to Phase 1. Tourmaline continued to continuously crystallize with Pyrite 2 and Pyrite 3, with a late mineral assemblage (muscovite, rutile, titanite; Kerrich and King, 1993). After the last pyrite overgrowth (Pyrite 3), pyrite fracturing and destabilization enabled the remobilization of gold and metals (Ag, Mo, Pb) into these fractures from the core (Pyrite 1) to the edges (Pyrite 3) and more rarely on the irregular surfaces of the cubic pyrite formed during Phase 3. This remobilization followed a late deformation of the region, probably Proterozoic, impacting the deposits, but not necessarily uniformly (Zhang et al., 2014 b). The Lac Herbin pyrite indicates remobilization, but fracturing is not observed in Goldex pyrite. This late remobilization at grain scale may account for the nuggety gold distribution observed in the deposits (Bonnemaison and Marcoux, 1990).

5.4. The three-stage evolution

We propose that each phase represents a particular redox environment, and that each pyrite growth stage (Pyrite 1, 2, and 3) represents a hydrothermal fluid pulse event (Fig. 8). Pyrite 1 formed during Phase 1 and the beginning of Phase 2. Phase 2 began with the formation of tourmaline and barite. Phase 3 then formed Pyrite 2, Pyrite 3, and tourmaline (barite only cristallized during Phase 2). Independent evidence for the three model is the observation that quartz in the QTC veins at the Lac Herbin deposit contains three types of successively-tapped fluid inclusions (Rezeau *et al.*, 2017): an early gold-bearing aqueous-carbonic fluid, a barren high-temperature moderately-saline aqueous fluid, and a barren low-temperature saline aqueous fluid. The first, gold-bearing fluid of Rezeau *et al.* (2017) corresponds to Phase 1, while the second, barren high-temperature fluid saline aqueous fluids, which would have remobilized gold in late fractures corresponding to the end of our Phase 3. The final, low-temperature fluid, is not recorded in the pyrite growth zones, and could be Proterozoic (Boullier et al., 1998).

5.5. *Tourmaline B-isotope variations and implications for fluid source*

The $\delta^{11}B$ values of tourmaline from all samples vary between -15.6 ‰ to -7.7 ‰, but the variation within a single deposit is on the order of 2-3 ‰ (Fig. 6C; Fig. 7). This narrow range is similar to results from a previous boron study in the district (Beaudoin *et al.*, 2013) but could be related to the small number of samples in this study (one per deposit and three for Lamaque). The Lamaque tourmalines are the exception in terms of a larger number of sample (n=3) and a larger range of values, from -14 to -9.1 ‰, while tourmaline from the Sigma deposit also yield a considerable range of $\delta^{11}B$ values, from -16.4 to -10.7‰ (Beaudoin *et al.*, 2013). Beaudoin *et al.* (2013) suggested that the large range $\delta^{11}B$ values at the Sigma deposit is caused by repetitive closed-reservoir tourmaline precipitation with a Rayleigh fractionation, followed by vein re-opening and the influx of new hydrothermal fluids during fault-valve cycles.

The $\delta^{11}B$ values suggest a spatial variation that divides the district into a southwest group

(Goldex and Lamaque), with values from -15.6 to -11.6 ‰, and a northeast group (Lac Herbin and Beaufor), with a higher range of $\delta^{11}B$ from -11.2 to -7.7 ‰ (Fig. 7). This divide in the district corresponds to a difference in the tourmaline Fe/Mg ratio, although, on the grain scale, the boron isotope composition is largely independent of the tourmaline chemical composition (this study and Beaudoin *et al.*, 2013). Tourmaline $\delta^{11}B$ values from Beaudoin *et al.* (2013) show the same spatial variation, with a southwest group (Sisco, Sigma, Audet, and Goldex) ranging between -15.5 to -11.6 ‰, and a northeast group (Orenada, Lucien Belliveau, Camnet-Nord, Buffadison, and Beaufor), with -12 to -9.5 ‰ (Fig. 6C). The highest $\delta^{11}B$ values (-9.5 to -7.7 ‰) are found close to large intrusions, such as Bourlamaque and the East Sullivan pluton (Fig. 7), but other locations in the eastern group also have high and are metavolcanic rocks (Lucien Béliveau and Buffadison). Futhermore, there are volcanic-hosted locations in the southwestern (Goldex, Sisco) with low $\delta^{11}B$ values (Fig. 7), so the nature of the host rocks does not exert a controlling influence.

In terms of boron reservoirs, the B-isotope values reported are too low to be compatible with an unmodified marine source ($\delta^{11}B > 0$ ‰; Chaussidon and Appell, 1997; Marschall and Jiang, 2011) or a subducting slab (from -5 ‰ to +28 ‰; Marschall *et al.*, 2009, Marocchi *et al.*, 2011). The B-isotope range is instead consistent with, but not diagnostic of, a greenstone source (i.e., MORB at -7 ± 1 ‰; Marschall *et al.*, 2017), with I-type intermediate magmas (-2 ± 5 ‰; Trumbull and Slack, 2018) or with clastic metamorphic rocks (prograde metamorphic tourmaline: -17‰ to +3 ‰, see Swihart and Moore, 1989; Jiang *et al.,* 2002). In any case, the observed ±8 ‰ range observed in Val-d'Or tourmaline cannot be explained by any one source type, and so requires a mixed fluid scenario, which is supported by the evidence of the discontinuous pyrite growth described above.

O-isotope thermometry from quartz-tourmaline pairs in the QTC veins at the Lamaque-Sigma deposit indicates a range of mineralization temperatures, ranging from approximately 350 to

450°C (Beaudoin and Pitre, 2005). Over this 100° C range, the tourmaline-fluid fractionation factors vary by about 1 ‰ (-3.2 ‰ and -2.3 ‰, resp.; using Meyer *et al.*, 2008), so the temperature effect on B isotope values is expected to be minor. Beaudoin and Pitre (2005) excluded temperature variations from explaining regional variations in $\delta^{18}O$, and proposed the contribution of more than one fluid with an average temperature of 350°C for the QTC veins. The calculated $\delta^{11}B$ range of hydrothermal fluids is approximately -12.4 ‰ to -4.5 ‰ (fractionation factors from Meyer *et al.*, 2008) which is supported by these new B-isotope values and those reported by Beaudoin *et al.* (2013). O-C-H and Sr- isotope ratios of the QTC veins suggest formation from a mixed fluid composed of two components: a prograde metamorphic fluid or a fluid thoroughly equilibrated with the metasedimentary and metavolcanic basement (Fluid 1), and a second fluid (Fluid 2) of supracrustal origin, with a possible marine source, trapped in pores and fractures (Beaudoin and Pitre, 2005; Beaudoin and Chiaradia, 2016). It is important to note that the $\delta^{18}O_{quartz}$ values from the Val-d'Or deposits are homogeneous within 11.5 ± 2.3 ‰ in the district, which suggests a decoupling of the boron and oxygen isotope systematics. These $\delta^{18}O_{quartz}$ values were attributed to a deep-seated metamorphic fluid source (Beaudoin and Pitre, 2005; Beaudoin and Chiaradia, 2016).

Our results support a metamorphic fluid source, and can be explained by a hydrothermal pulse of deep-seated metamorphic fluid (Fluid 1) that rose into the fault system and infiltrated a shallow crustal portion already saturated by an oxidized, B-bearing supracrustal fluid (Fluid 2). This oxidized B-bearing fluid is recorded by the occurance of barite and a positive Eu anomaly in coexisting tourmaline. At the end of the hydrothermal pulse (Fluid 1), the barren supracrustal fluid became dominant. It changed the redox condition of the environment and, for still unknown reason, stopped gold mineralization (Phase 2). This supracrustal fluid (Fluid 2) could be an evolved metamorphic fluid, which would have interacted with B- and Ba-rich lithologies, such as metasediments, during its rising in the CLLFZ, or a saline supracrustal fluid in the fault

system. The $\delta^{11}B$ fluid values of approximately -12 to -6 ‰ are consistent with a prograde metamorphic fluid from metasedimentary and metavolcanic rocks. The higher $\delta^{11}B$ fluid values may be explained by mixing with a second fluid. A marine-derived pore fluid, as suggested by earlier studies, would be an excellent source of boron and sulfate, and consistent with the formation of barite and tourmaline. Contemporary to the QTC veins, the marine water source could be linked to the Timiskaming assemblage at 2678-2672 Ma (Davis, 2002). However, even the highest $\delta^{11}B$ fluid value, of -4.5 ‰, is too low for an unmodified marine-sourced fluid. The original B-isotope composition of pore fluid could be modified by later processes related to diagenesis and metamorphism, but a shift of approximately 20 ‰ would require very extensive exchange with boron in the host rocks. The other, perhaps more likely, hypothesis is that the end-member marine B-isotope signature of Fluid 2 was diluted in the mixed fluid. All that can be concluded with confidence is that isotopically light and heavy fluids contributed to the hydrothermal fluid from which the tourmaline formed. If one fluid had a marine origin, the B-isotope data require that its $\delta^{11}B$ signature was then modified by extensive exchange with the host rock or that it was diluted by the dominant, isotopically lighter, metamorphic fluid.

Concerning the spatial variation, the B-isotope values suggest a difference in fluid proportions in the different parts of the district, which could be caused by varying proximity to the main or subsidiary fault zones that control the hydrodynamics of the system (Beaudoin and Pitre, 2005). Depending on a deposit's location in the district, tourmaline and barite could have formed early in the vein system.

6. Conclusions

The Val-d'Or mining district remains a key example for understanding of orogenic gold deposit formation processes. The QTC veins across the district resulted from a multi-stage hydrothermal event that took place over a maximum 114 Ma period, between 2680 Ma (Wong

et al., 1991) and 2566 ±71 Ma (Olivo *et al.*, 2007), after the end of the Superior Province accretion (Fig. 8). These results support a three-stage evolution for the QTC vein field. In Phase 1, gold mineralization took place early in the QTC vein field formation, in the third-order faults of the CLLFZ. Gold formed during the first hydrothermal pulse, forming disseminated inclusions in the pyrite, alloyed with variable proportions of silver and tellurium, and also as pure gold inclusions. This first fluid pulse involved deep-seated, reduced metamorphic fluids that infiltrated into a shallow crustal segment that was already saturated with an oxidized B-bearing supracrustal fluid. In Phase 2, the waning of the deep-seated fluid pulse enabled the supracrustal fluid to become dominant and this produced a change in the redox conditions, from reduced to oxidized, caused the precipitation of tourmaline and barite, and ended gold mineralization. This supracrustal fluid impacted the entire district, but mixing ratios varying with depth, location in the district, and the interaction time. The different mixing ratios are recorded by variability in the $\delta^{11}B$ signature of in tourmaline, which range from -15.6 ‰ to -7.7 ‰. The mixing ratio and B isotopic variation are not related to the host rock, but rather to their proximity to the main or subsidiary fault zones. Phase 3 involved a new pulse of reduced hydrothermal fluid and/or a decreased proportion of the supracrustal fluid, resulting in a change of fluid conditions from oxidized to reduced. Non-auriferous pyrite crystallized around Pyrite 1, tourmaline and barite, with a slower growth rate and Co-As-Ni-rich zonation (Pyrite 2 and 3). Tourmaline crystallization continued in those veins with pyrite and quartz but without barite. This three-stage evolution of the Val-d'Or vein field, with the mixing of deep-seated and supracrustal fluids, provides a new perspective to understand polyphase orogenic gold deposits worldwide.

ACKNOWLEDGMENTS

We are grateful to the FRQNT and NSERC for the funding of this project. We thank Frederic Couffignal for expert assistance with the SIMS analysis at GFZ and Brandon Boucher for element mapping analysis. Reynald Lapointe, Christian Sasseville, and Anna Jung are thanked for their technical help. Thanks also to Stéphane de Souza and Vincent Van Hinsberg for their helpful comments and discussions during this work, and to Daniele Pinti for his great help in comments and suggestions to improve the manuscript. We thank the reviewers for their very constructive feedback.

References

Beaudoin, G. and Pitre, D., 2005, Stable isotope geochemistry of the Archean Val-d'Or (Canada) orogenic gold vein field. Mineralium Deposita*, v. 40*, p. 59-75.

Beaudoin G., Rollion-Bard, C., and Giuliani, G., 2013, The boron isotope composition of tourmaline from the Val-d'Or orogenic gold deposits, Québec, Canada. Mineral Deposit Research For A High-Tech World. 12th SGA Biennial Meeting, Proceedings, v. 3, p. 1090-1092.

Beaudoin, G. and Chiaradia, M., 2016, Fluid mixing in orogenic gold deposits: Evidence from the HO-Sr isotope composition of the Val-d'Or vein field, Abitibi, Canada. Chemical Geology, v. *437*, p. 7-18.

Beauregard, A.J., Gaudreault, D. and D'Amours, C. 2014. NI 43 101 Technical Report on the Lamaque property. Technical report prepared by Geologica Groupe-Conseil Inc. for Integra Gold Corp. 101 pages.

Bonnemaison, M., & Marcoux, E. (1990). Auriferous mineralization in some shear-zones: A three-stage model of metallogenesis. Mineralium Deposita, 25(2), 96-104.

Boullier, A. M., and Robert, F., 1992, Palaeoseismic events recorded in Archean gold-quartz vein network, Val-d'Or, Abitibi, Quebec, Canada. Journal of Structural Geology, v. 14(2), p. 161-179

Boullier, A. M., Firdaous, K., & Robert, F. (1998). On the significance of aqueous fluid inclusions in gold-bearing quartz vein deposits from the southeastern Abitibi subprovince (Quebec, Canada). Economic Geology, 93(2), 216-223.

Card, K. D., & Ciesielski, A., 1986, DNAG# 1. Subdivisions of the Superior province of the Canadian shield. Geoscience Canada, v.13(1).

Catanzaro, E.J., Champion, C., Garner, E., Marinenko, G., Sappenfield, K., Shields, W., 1970, Boric

acid: isotopic and assay standard reference materials. National Bureau of Standards (US), Special Publication, v. 260, p. 70.

Chaussidon, M., and Appel, P. W. U., 1997, Boron isotopic composition of tourmalines from 3.8-Ga-old Isua supreacrustals, West Greenland: implication of the $\delta^{11}B$ value of early Archean seawater. Chemical Geology, v. 136(3-4), p. 171-180.

Couture, J. F., Pilote, P., Machado, N., & Desrochers, J. P., 1994, Timing of gold mineralization in the Val-d'Or District, southern Abitibi Belt; evidence for two distinct mineralizing events. Economic Geology, v. 89(7), p. 1542-1551.

Davis, D. W. (2002). U–Pb geochronology of Archean metasedimentary rocks in the Pontiac and Abitibi subprovinces, Quebec, constraints on timing, provenance and regional tectonics. Precambrian Research, 115(1-4), 97-117.

Dutrow, B.L. and Henry, D.J., 2011, Tourmaline: a geologic DVD: Elements, v. *7*(5), p. 301-306.

Feng, R. and Kerrich, R., 1992, Geochemical evolution of granitoids from the Archean Abitibi Southern Volcanic Zone and the Pontiac subprovince, Superior Province, Canada: implications for tectonic history and source regions: Chemical Geology, v. 98(1-2), p. 23-70.

Fontaine, A., Eglinger, A., Ada, K., André-Mayer, A. S., Reisberg, L., Siebenaller, L., & Poujol, M. (2017). Geology of the world-class Kiaka polyphase gold deposit, West African Craton, Burkina Faso. Journal of African Earth Sciences, 126, 96-122.

Gaboury, D., 1999, Origine volcanogène des veines aurifères riches en sulfures de la mine Géant Dormant, Abitibi, Québec: Université du Québec à Chicoutimi.

Genest, R., 2012. Technical Report on the Estimation of the Mineral Resources at Goldex Mine, Quebec, Canada as at December 31, 2011. 102p.

Goldfarb, R. J., & Groves, D. I., 2015, Orogenic gold: Common or evolving fluid and metal sources through time. Lithos, v. 233, p. 2-26.

Green, A. G., Milkereit, B., Mayrand, L. J., Ludden, J. N., Hubert, C., Jackson, S. L., and Simard, A., 1990, Deep structure of an Archean greenstone terrane: Nature, v. 344(6264), p. 327.

Hanes, J.A., Archibald, D. A., Hodgson, C. J. and Robert, F., 1992, Dating Archean auriferous quartz vein deposits in the Abitibi greenstone belt, Canada: $^{40}Ar/^{39}Ar$ evidence for a 70- to 100-My-time gap between plutonism-metamorphism and mineralization: Economic Geology, v. 87(7), p. 1849-1861.

Henry, D.J., Novak, M., Hawthorne, F.C., Ertl, A., Dutrow, B.L., Uher, P. and Pezzotta, F., 2011, Nomenclature of the tourmaline-supergroup minerals: American Mineralogist, v. 96(5-6), p. 895-913.

Jemielita, R., Davis, D. and Krogh, T., 1990, U-Pb evidence for Abitibi gold mineralization postdating

greenstone magmatism and metamorphism: Nature, v. 346(6287), p. 831.

Jiang, S. Y., Palmer, M. R., and Yeats, C. J., 2002, Chemical and boron isotopic compositions of tourmaline from the Archean Big Bell and Mount Gibson gold deposits, Murchison Province, Yilgarn craton, Western Australia. Chemical Geology, v. 188(3-4), p. 229-247.

Kerrich, R. and King, R., 1993, Hydrothermal zircon and baddeleyite in Val-d'Or Archean mesothermal gold deposits: characteristics, compositions, and fluid-inclusion properties, with implications fortiming of primary gold mineralization: Canadian Journal of Earth Sciences, v. 30(12), p. 2334-2351.

Kerrich, R. and Ludden, J., 2000, The role of fluids during formation and evolution of the southern Superior Province lithosphere: an overview: Canadian Journal of Earth Sciences, v. 37(2-3), p. 135-164.

Krienitz, M.-S., Trumbull, R.B., Hellmann, A., Kolb, J., Meyer, F.M., Wiedenbeck, M., 2008, Hydrothermal gold mineralization at the Hira Buddini Gold Mine, India: contraints on fluid sources and evolution from boron isotopic compositions of tourmaline. Mineralium Deposita, v. 43, p. 421-434.

Lambert-Smith, J.S., Rocholl, A., Treloar, P.J., Lawrence, D.M., 2016, Discriminating fluid source regions in orogenic gold deposits using B-isotopes. Geochimica et Cosmochimica Acta, v. 194, p. 57-76.

Large, R.R., Danyushevsky, L., Hollit, C., Maslennikov, V., Meffre, S., Gilbert, S., Bull, S., Scott, R., Emsbo, P. and Thomas, H., 2009, Gold and trace element zonation in pyrite using a laser imaging technique: implications for the timing of gold in orogenic and Carlin-style sediment-hosted deposits: Economic Geology, v. 104(5), p. 635-668.

Latulippe, M., 1966, The relationship of mineralization to Precambrian stratigraphy in the Matagami Lake and Val-d'Or districts of Quebec: Geological Association of Canada, v. 3, p. 21-42.

Lemarchand, J. (2012). Les minéralisations filoniennes aurifères du pluton de Bourlamaque (Val-d'Or, Abitibi): synthèse structurale et apports de la datation 40AR/39AR (Doctoral dissertation, Université du Québec à Montréal).

Marocchi, M., Marschall, H.R., Konzett, J., Tropper, P., Ludwig, T., Mair, V. and Bargossi, G.M., 2011, Metasomatic tourmaline in hybrid contact-bands between gneiss and peridotite in the Ulten zone of the Eastern Italian Alps: chemistry and boron isotopic composition: The Canadian Mineralogist, v. 49(1), p. 245-261.

Marschall, H.R., Meyer, C., Wunder, B., Ludwig, T. and Heinrich, W., 2009, Experimental boron isotope fractionation between tourmaline and fluid: confirmation from in situ analyses by secondary ion mass spectrometry and from Rayleigh fractionation modelling: Contributions to

Mineralogy and Petrology, v. 158(5), p. 675-681.

Marschall, H.R. and Jiang, S.-Y., 2011, Tourmaline isotopes: no element left behind: Elements, v. 7(5), p. 313-319.

Marschall, H.R., Wanless, V.D., Shimizu, N., Pogge von Strandmann, P.A.E., Elliott, T., Monteleone, B.D., 2017, The boron and lithium isotopic composition of mid-ocean ridge basalts and the mantle. Geochimica et Cosmochimica Acta, v. 207, p. 102–138.

McDonough, W.F. and Sun, S.-S., 1995, The composition of the Earth: Chemical geology, v. 120(3-4), p. 223-253.

Mériaud, N., & Jébrak, M. (2017). From intrusion-related to orogenic mineralization: the Wasamac deposit, Abitibi Greenstone Belt, Canada. Ore Geology Reviews, 84, 289-308.

Meyer, C., Wunder, B., Meixner, A., Romer, R. L., & Heinrich, W., 2008, Boron-isotope fractionation between tourmaline and fluid: an experimental re-investigation. Contributions to Mineralogy and Petrology, v. 156(2), p. 259-267.

Molnár, F., Middleton, A., Stein, H., Hugh, O., Lahaye, Y., Huhma, H., & Johanson, B. (2018). Repeated syn-and post-orogenic gold mineralization events between 1.92 and 1.76 Ga along the Kiistala Shear Zone in the Central Lapland Greenstone Belt, northern Finland. Ore Geology Reviews, 101, 936-959.

Murowchick, J.B. and Barnes, H., 1987, Effects of temperature and degree of supersaturation on pyrite morphology: American Mineralogist, v. 72(11-12), p. 1241-1250.

Neumayr, P., Hagemann, S.G., 2002, Hydrothermal fluid evolution within the Cadillac tectonic zone, Abitibi greenstone belt, Canada: relationship to auriferous fluids in adjacent second- and third-order shear zones. Economic Geology, v. 97, p. 1203–1225

Pilote, P., Mueller, W., Scott, C., Lavoie, S., Champagne, C. and Moorhead, J., 1998, Volcanologie de la formation de Val-d'Or et du Groupe de Malartic, sous-Province de l'Abitibi: contraintes géochimiques et géochronologiques : Ministère des Ressources naturelles du Québec, DV, p. 98-05.

Rafini, S., 2014. Typologie des minéralisations aurifères associées à la Faille de Cadillac. Rapport du projet CONSOREM 2011-01 et 2012-01, 45 p.

Rezeau, H., Moritz, R., & Beaudoin, G., 2017, Formation of Archean batholith-hosted gold veins at the Lac Herbin deposit, Val-d'Or district, Canada: Mineralogical and fluid inclusion constraints. Mineralium Deposita, v. 52(3), p. 421-442.

Robert, F. and Brown, A.C., 1986, Archean gold-bearing quartz veins at the Sigma Mine, Abitibi greenstone belt, Quebec; Part I, Geologic relations and formation of the vein system: Economic Geology, v. 81(3), p. 578-592.

Robert, F., 1990, Structural setting and control of gold-quartz veins of the Val-d'Or area, southeastern Abitibi subprovince: Gold and base metal mineralization in the Abitibi Sub-Province, Canada, with Emphasis of the Quebec Segment. Geology Department (Key Centre) and University Extension, the University of Western Australia. Publication No. 24, 167-210.

Robert, F., 1994, Vein fields in gold districts: The example of Val-d'Or, southeastern Abitibi subprovince. Quebec: Geological Survey of Canada, Current Research Paper, p. 295-302.

Robert, F., Poulsen, K.H., Cassidy, K.F., and Hodgson, C.J., 2005, Gold metallogeny of the Superior and Yilgarn cratons: ECONOMIC GEOLOGY 100TH ANNIVERSARY VOLUME, p. 1001–1033.

Román, N., Reich, M., Leisen, M., Morata, D., Barra, F., & Deditius, A. P. (2019). Geochemical and micro-textural fingerprints of boiling in pyrite. Geochimica et Cosmochimica Acta, 246, 60-85.

Scott, C.R., Mueller, W.U. and Pilote, P., 2002, Physical volcanology, stratigraphy, and lithogeochemistry of an Archean volcanic arc: evolution from plume-related volcanism to arc rifting of SE Abitibi Greenstone Belt, Val-d'Or, Canada: Precambrian Research, v. 115(1), p. 223-260.

Sibson, R. H., Moore, J. M. M., & Rankin, A. H., 1975, Seismic pumping—a hydrothermal fluid transport mechanism: Journal of the Geological Society, v. 131(6), p. 653-659.

Sibson, R.H., Robert, F. and Poulsen, K.H., 1988, High-angle reverse faults, fluid-pressure cycling, and mesothermal gold-quartz deposits: Geology, v. 16(6), p. 551-555.

Swihart, G.H. and Moore, P.B., 1989, A reconnaissance of the boron isotopic composition of tourmaline: Geochimica et Cosmochimica Acta, v. 53(4), p. 911-916.

Trumbull, R.B., Slack, J.F., 2018, Boron isotopes in the continental crust: granites, pegmatites, felsic volcanic rocks and related ore deposits. In: Marschall, H.R., Foster, G.L. (Eds) Boron Isotopes - The Fifth Element. Advances in Geochemistry, Springer, Heidelberg, v. 7, p. 249-272.

Van Hinsberg, V. J., and Schumacher, J.C., 2009, The geothermobarometric potential of tourmaline, based on experimental and natural data: American Mineralogist, v. 94(5-6), p. 761-770.

Wang, L., Shi, X., & Jiang, G., 2012, Pyrite morphology and redox fluctuations recorded in the Ediacaran Doushantuo Formation. Palaeogeography, Palaeoclimatology, Palaeoecology, v. 333, p. 218-227.

Wong, L., Davis, D., Krogh, T. and Robert, F., 1991, UPb zircon and rutile chronology of Archean greenstone formation and gold mineralization in the Val-d'Or region, Quebec: Earth and Planetary Science Letters, v. 104(2-4), p. 325-336.

Zhang, J., Deng, J., Chen, H.-Y., Yang, L.-Q., Cooke, D., Danyushevsky, L. and Gong, Q.-J., 2014a, LA-ICP-MS trace element analysis of pyrite from the Chang'an gold deposit, Sanjiang region,

China: Implication for ore-forming process: Gondwana Research, v. 26(2), p. 557-575.

Zhang, J., Linnen, R., Lin, S., Davis, D., & Martin, R., 2014b. Paleoproterozoic hydrothermal reactivation in a Neoarchean orogenic lode-gold deposit of the southern Abitibi subprovince: U-Pb monazite geochronological evidence from the Young-Davidson mine, Ontario. Precambrian Research, 249, 263-272.

FIGURE CAPTIONS

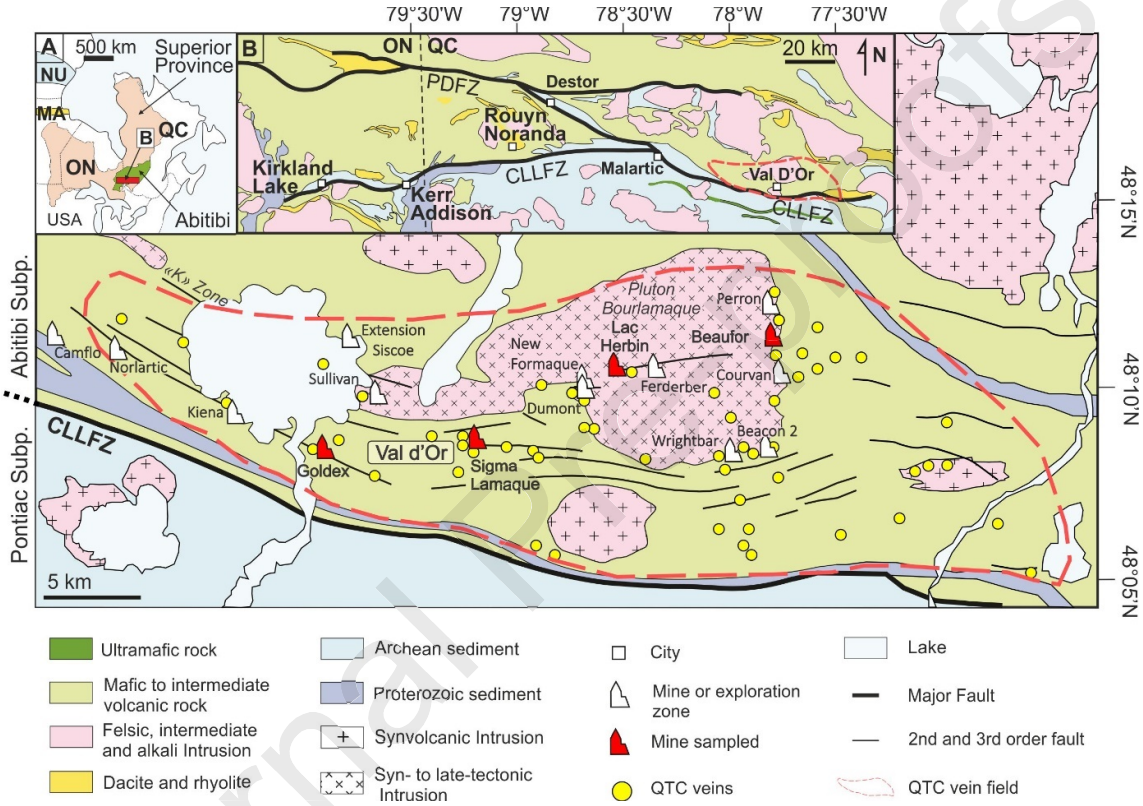

Figure 1. Simplified map of the Abitibi Greenstone Belt and the Val-d'Or mining district (modified from Neumayr and Hagemmann (2002), Robert *et al.* (2005), and Mériaud and Jébrak (2017)). Red symbols of a mine shaft represent mines sampled as part of this study, which all exploit quartz-tourmaline-carbonate (QTC) auriferous veins, represented by yellow circles. ON = Ontario, QC = Quebec, CLLFZ = Cadillac-Larder Lake fault zone, and PDFZ = Porcupine-Destor fault zone.

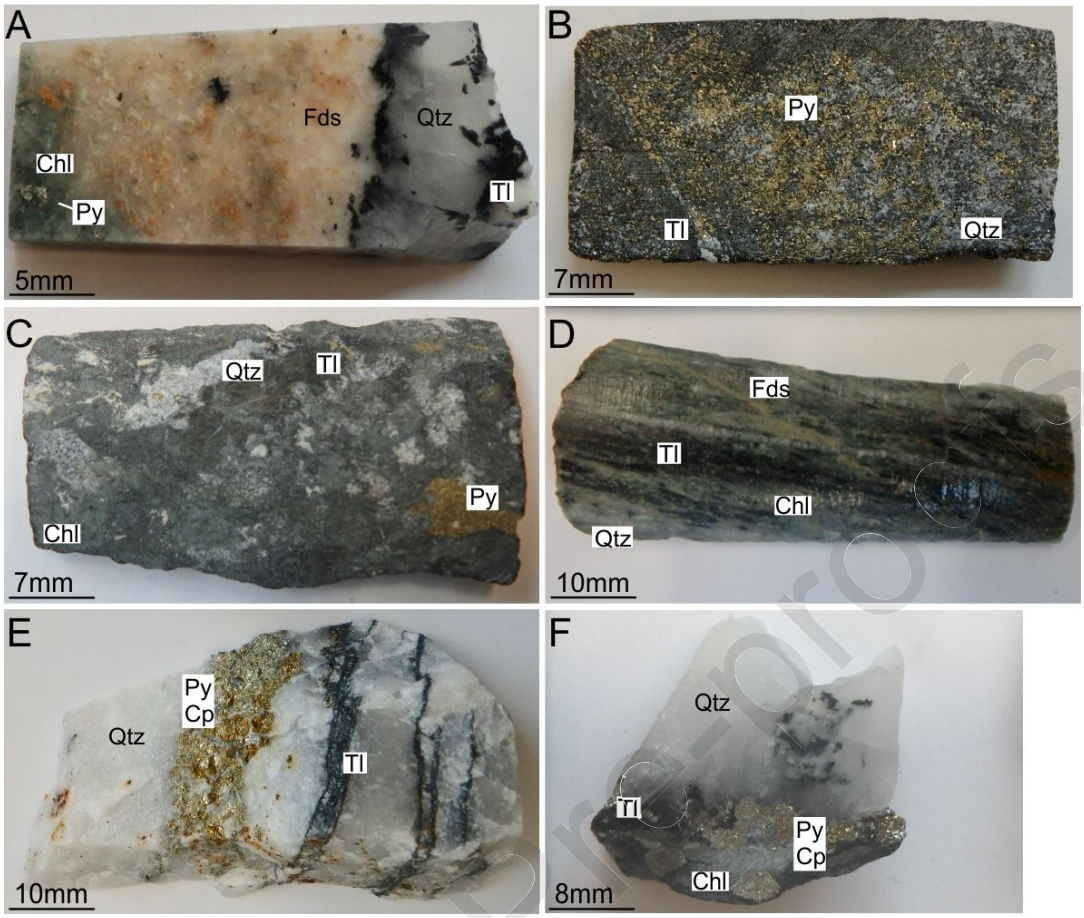

Figure 2: Hand sample pictures of investigated vein samples. (A) quartz-tourmaline vein with pyrite, K-feldspar, and chlorite in sample 91 from a Goldex mine drill core, (B) quartz-tourmaline vein with disseminated pyrite in sample 88 from the Lamaque parallel exploration zone drill core, (C) quartz-tourmaline vein with pyrite and chlorite in sample 85, (D) quartz-tourmaline vein with chlorite and feldspar veinlets in sample 87 from the same Lamaque triangle exploration zone drill core, (E) quartz-tourmaline vein with pyrite and chalcopyrite from the Lac Herbin mine, and (F) quartz-tourmaline vein with pyrite, chalcopyrite, and chlorite from the Beaufor mine. Py = pyrite, Chl = chlorite, Fds = feldspath, Qtz = quartz, Tl = tourmaline, and Cp = chalcopyrite.

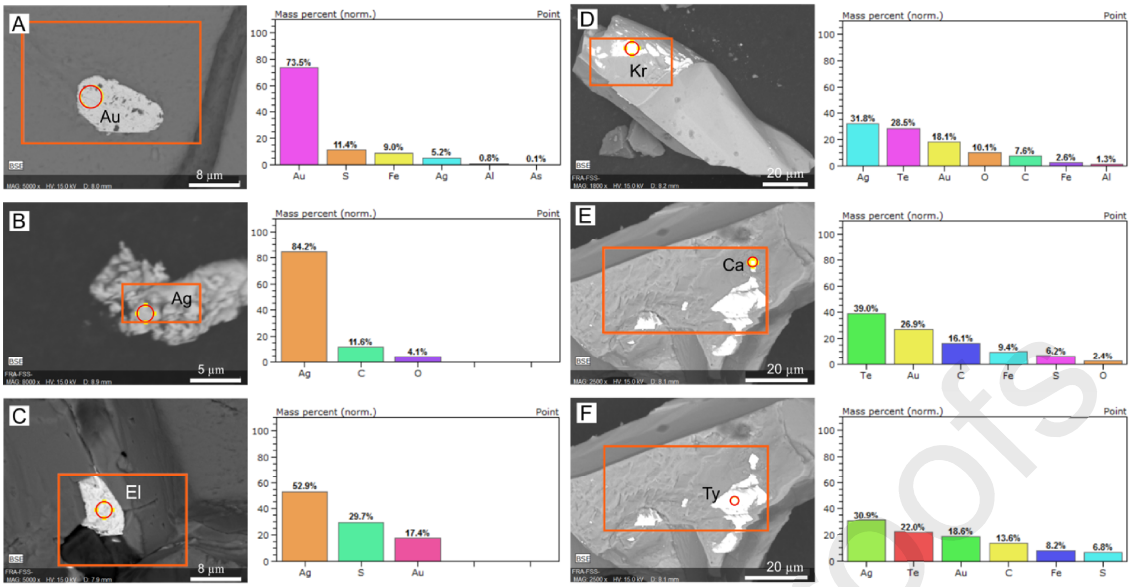

Figure 3. BSE-SEM photomicrographs of regions analyzed by SEM-EDX from Val-d'Or deposit sample grains. The red circle indicates with precision the area analyzed. From Lamaque, analysis of A) gold (Au), B) native silver (Ag), C) electrum (Ag, Au), D) krennerite (Au_3AgTe_8) as inclusions in different pyrite grains, E) calaverite ($AuTe_2$), and F) tetradymite (Bi_2Te_2S) in inclusions in the same pyrite grain. The carbon content is related to the epoxy mounts which hold the grains. Sulfur and iron contents are related to the pyrite which hosts the inclusions. Au = gold, Ag = silver, El = electrum, Kr = krennerite, Ca = calaverite, and Ty = tetradymite.

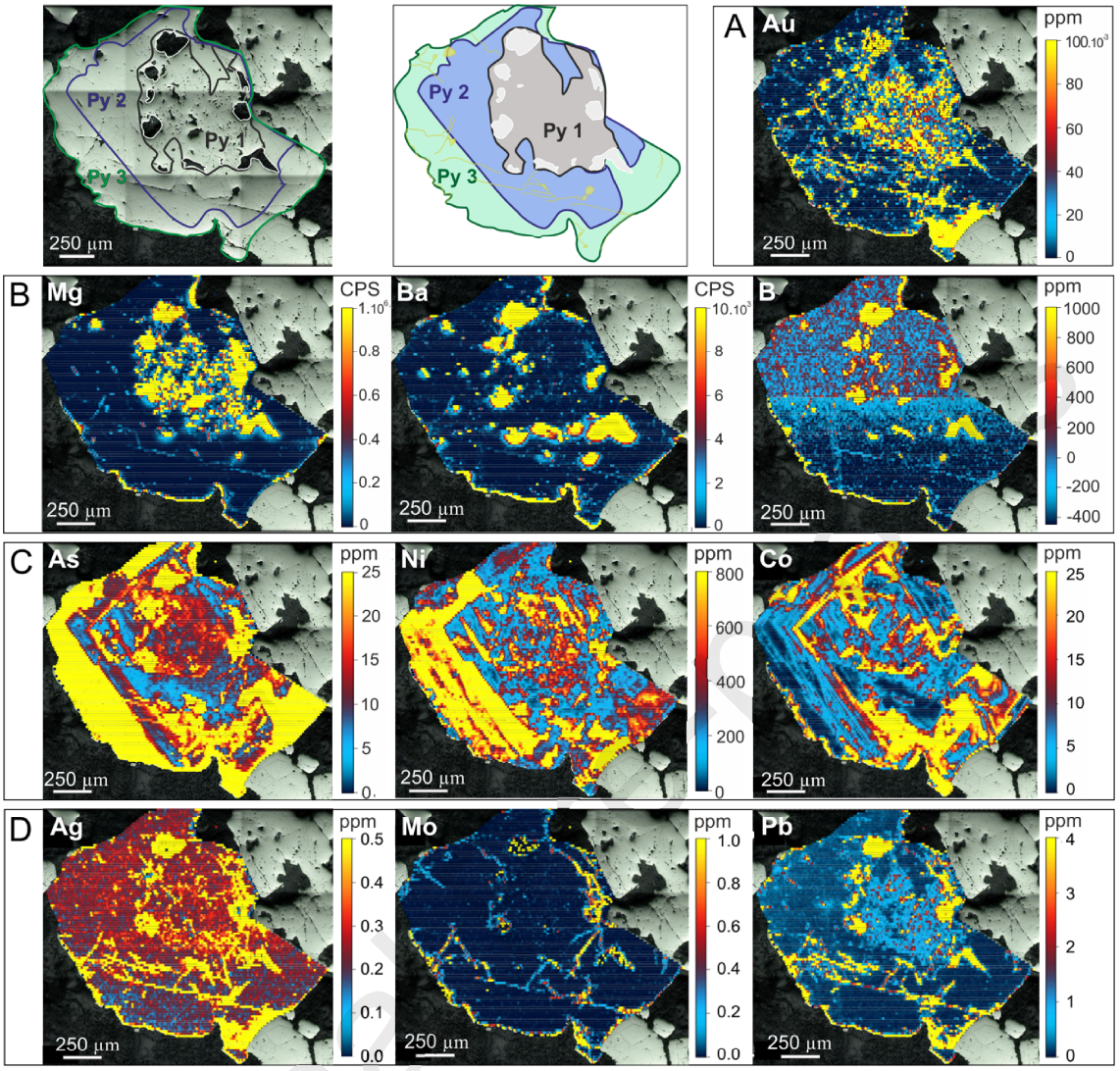

Figure 4. Element mapping of Au, Mg, Ba, B, As, Ni, Co, Ag, Mo and Pb by LA-ICP-MS on polyphased pyrite grain from the Lac Herbin deposits. In the Lac Herbin pyrite, A) Au occurs as inclusions in the core and is remobilized in late fractures (Au accumulation at the bottom of Pyrite 3 is an effect of saturation in the fracture), B) while Mg is present only in the core in the inclusions. Ba and B are concentrated in inclusions at the margin of Pyrite 1 and 2, and in the dissolution halo of Pyrite 3. C) Pyrite 2 is Co-rich. As and Ni concentrations suggest a zoning pattern, which forms cubic Pyrites 2 and 3. Pyrite 3 is particularly As-Ni-rich. D) Ag, Mo, and Pb are concentrated in the fractures, indicating remobilization.

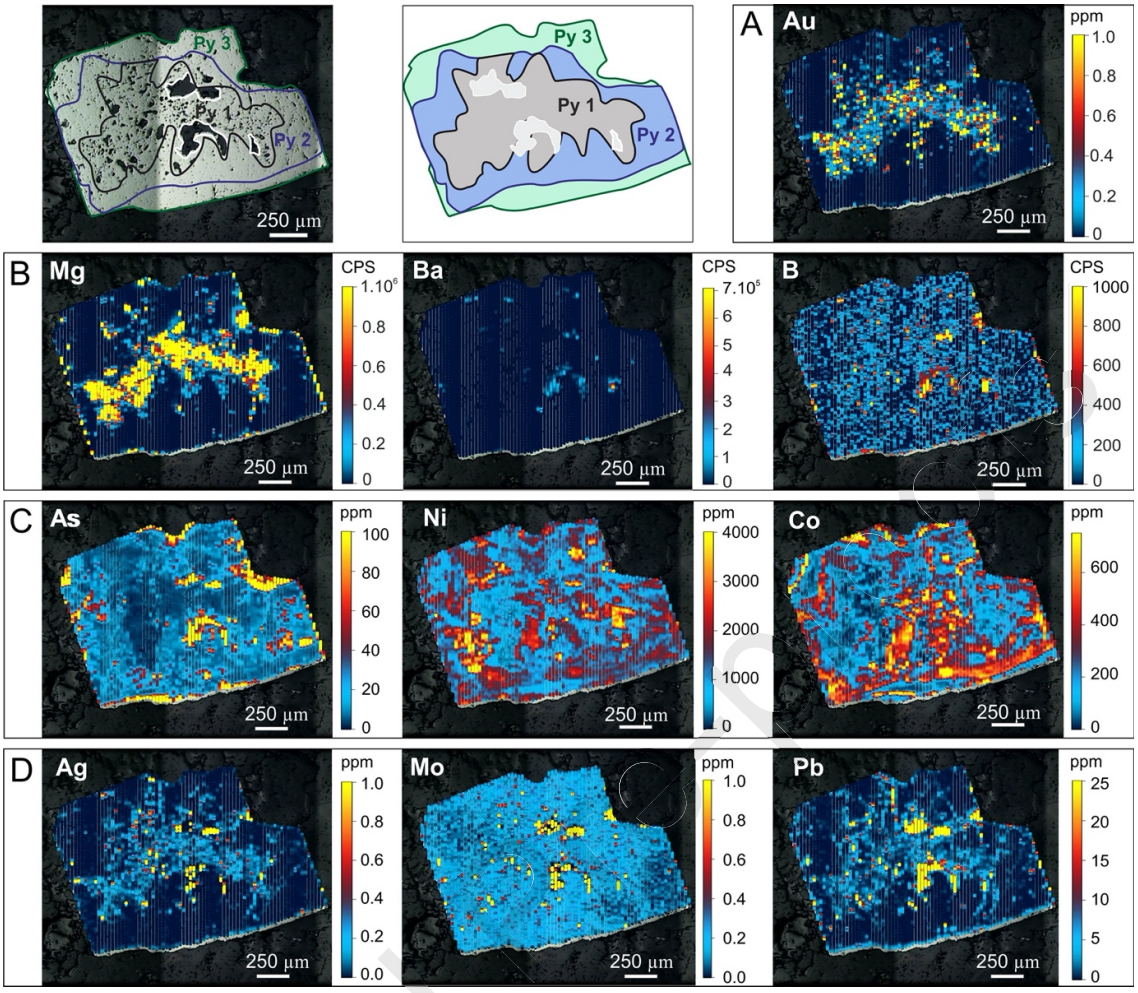

Figure 5. Element mapping of Au, Mg, Ba, B, As, Ni, Co, Ag, Mo, and Pb by LA-ICP-MS on polyphased pyrite grain from Goldex deposits. The white rim represents the edge of the pyrite. In the Goldex pyrite, A) Au and B) Mg are concentrated in micro-inclusions in the core of Pyrite 1. Au concentrations reach 1 ppm. B) Ba and B are more important than in the Lac Herbin pyrite, and are concentrated in inclusions in the Pyrite 1 dissolution halo, at the outer grain boundary.C) Pyrite 2 is Co-rich. As and Ni concentrations are higher than in Lac Herbin pyrite and also suggest a zoning pattern in the outer part of the pyrite, indicating Pyrite 3 (As-rich). D) There is no indication of fracture and metal remobilization.

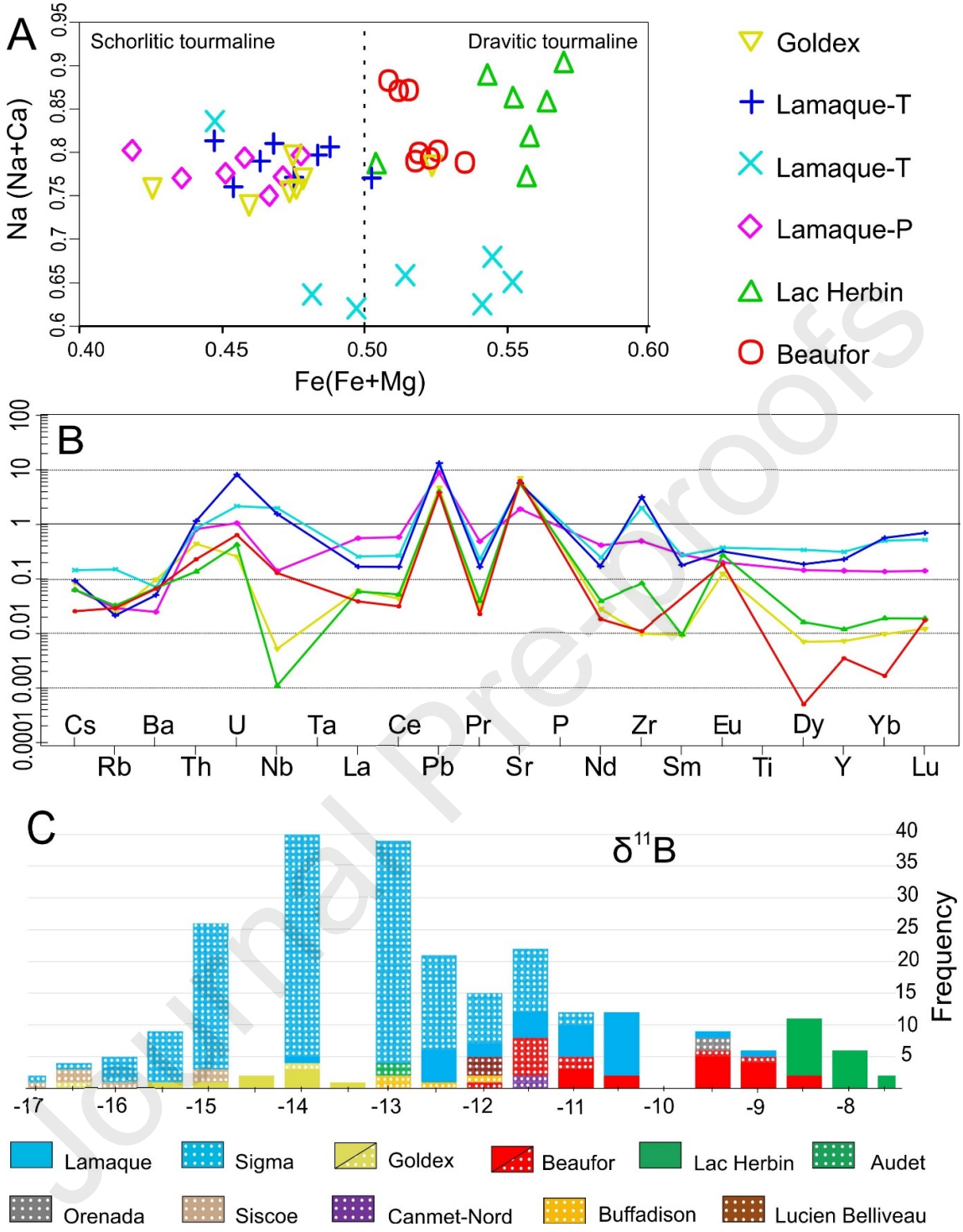

Figure 6. Geochemical analyses of select Val-d'Or tourmalines. A) Mg/(Fe+Mg) vs. Na/(Na+Ca) variations in Val-d'Or tourmaline, with schorl-dravite nomenclature. B) Val-d'Or tourmaline average trace element compositions plotted on a primitive mantle-normalized diagram (mantle values from McDonough and Sun (1995)). C) Val-d'Or tourmaline $\delta^{11}B$ values in ‰ (analytical error is ± 0.6 ‰, 1 sd). The dotted bars are values from Beaudoin *et al.* (2013).

For the Lamaque deposit, the $\delta^{11}B$ values combine data from the Triangle and Parallel zone samples. Sigma and Lamaque deposits are geographically close and geochemically related. The Audet deposit shares the same structure as the Lac Herbin deposit.

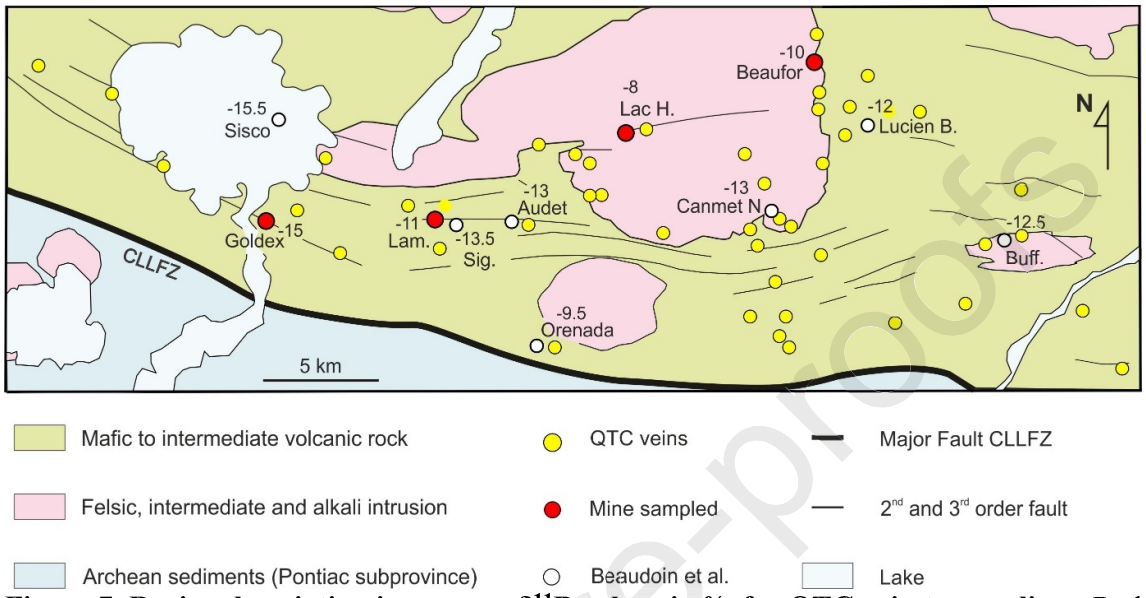

Figure 7. Regional variation in average $\delta^{11}B$ values in ‰ for QTC vein tourmalines. Red dots represent locations corresponding with boron isotope analysis from this study and white dots represent those from Beaudoin *et al.* (2013). Lam. = Lamaque, Sig. = Sigma, Lucien B. = Lucien Belliveau, and Buff. = Buffadison.

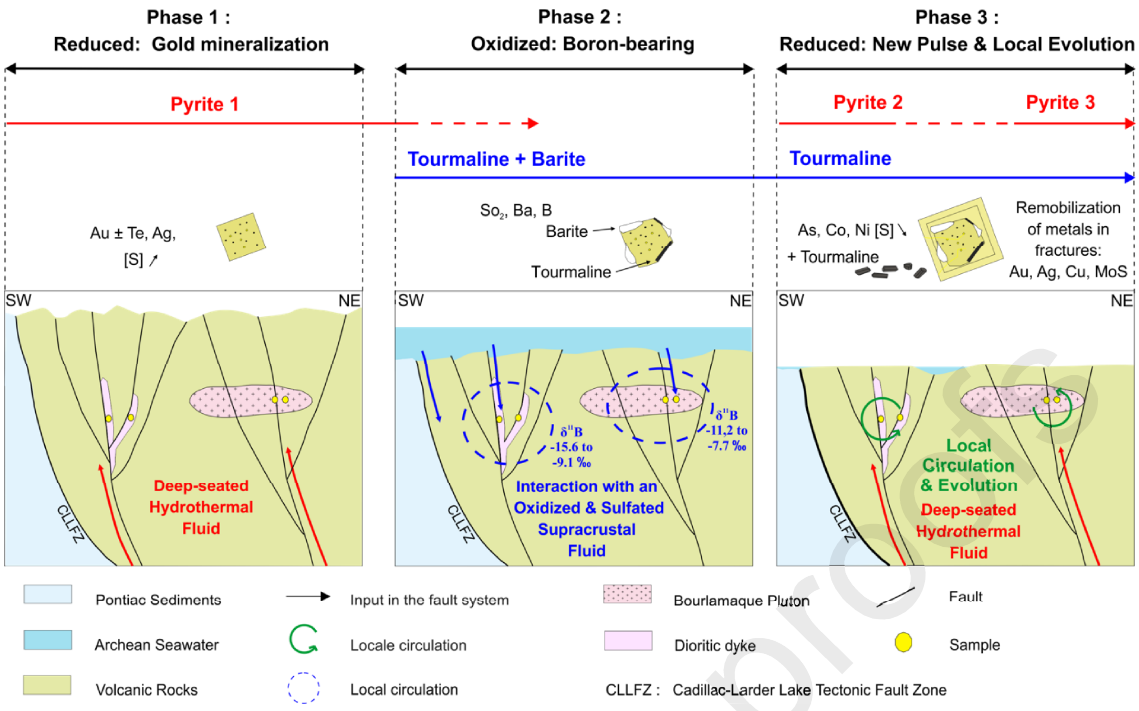

Figure 8. Suggested scenario for quartz-tourmaline-carbonate vein evolution. Phase 1 represents the formation of gold-bearing pyrite from a deep-seated fluid under reducing conditions. Phase 2 involves mixing with an oxidized and supracrustal fluid, indicated by the dissolution of pyrite and the crystallization of barite and tourmaline. Phase 3 corresponds to a return to reducing conditions with the formation of non-auriferous As-Co-Ni-rich cubic pyrite, arsenopyrite, and tourmaline. Yellow circles represent the locations of the sampled QTC veins.

Table 1. Mineralogy of the Val-d'Or quartz-carbonate-tourmaline veins.

		Goldex	Lam. Parallel	Lam. Triangle	Lac H.	Beaufor
Pyrite Habit	Cubic Sub-euhedral Anhedral					
Metal inclusions in pyrite or isolated	Gold (Au) Silver (Ag) Electrum (Au,Ag)					
Tellurium	Tellurobismuthite Calaverite ($AuTe_2$) Krennerite (Au_3AgTe_8) Tetradymite (Bi_2Te_2S)					
Tourmaline	Schorl Uvite Dravite					
Barite						
Sulfides	Pyrrhotite (Fe_7S_8) Chalcopyrite ($CuFeS_2$) Molybdenite (MoS)					
	Arsenopyrite (FeAsS)					
Quartz						
Carbonate	Calcite Dolomite					
Feldspar	Albite Microcline (K-feldspar)					
Mica	Biotite Muscovite					
Titanite Scheelite Chlorite Rutile Hematite Apatite						
Zircon						

> 50% of the assemblage

Major mineral in the assemblage

Minor mineral in the assemblage

Table 2. Summary of SIMS B-isotope analyses of select tourmalines.

Analysis	$^{11}B/^{10}B$ (meas.)	int. precision*	$^{11}B/^{10}B$ (corr.)**	$\delta^{11}B$***
Beaufor tourmalines from one sample				
Beaufor 1	3.925	0.13	4.0067	-9.1
Beaufor 2	3.9259	0.1	4.0076	-8.9
Beaufor 3	3.9261	0.1	4.0078	-8.9
Beaufor 4	3.9235	0.12	4.0051	-9.5
Beaufor 5	3.9239	0.12	4.0055	-9.4
Beaufor 6	3.9175	0.12	3.999	-11
Beaufor 7	3.9173	0.16	3.9987	-11.1
Beaufor 8	3.9231	0.1	4.0047	-9.6
Beaufor 9	3.9243	0.11	4.0059	-9.3
Beaufor 10	3.9229	0.09	4.0045	-9.7
Beaufor 11	3.923	0.13	4.0046	-9.6
Beaufor 12	3.924	0.12	4.0056	-9.4
Beaufor 13	3.918	0.15	3.9995	-10.9
Beaufor 14	3.9168	0.15	3.9983	-11.2
Beaufor 15	3.9195	0.15	4.001	-10.5
Beaufor 16	3.9228	0.16	4.0044	-9.7
Beaufor 19 05	3.8293	0.21	3.9993	-10.9
			Mean	**-9.9**
			St. dev.	**0.7**
Lac Herbin tourmalines from one sample				
LacHerbin 1	3.9276	0.1	4.0093	-8.5
LacHerbin 2	3.9294	0.09	4.0112	-8,0
LacHerbin 3	3.9297	0.09	4.0114	-8,0
LacHerbin 4	3.9276	0.1	4.0093	-8.5
LacHerbin 5	3.9243	0.09	4.0059	-9.3
LacHerbin 6	3.9275	0.12	4.0091	-8.5
LacHerbin 7	3.9271	0.14	4.0088	-8.6
LacHerbin 8	3.9272	0.1	4.0089	-8.6
LacHerbin 9	3.9299	0.13	4.0116	-7.9
LacHerbin 10	3.9257	0.13	4.0073	-9,0
LacHerbin 11	3.9307	0.12	4.0125	-7.7
LacHerbin 12	3.9273	0.1	4.0089	-8.6
LacHerbin 13	3.928	0.14	4.0097	-8.4
LacHerbin 14	3.928	0.07	4.0097	-8.4
LacHerbin 15	3.9257	0.13	4.0073	-9,0
LacHerbin 16	3.9265	0.16	4.0082	-8.8
LacHerbin 17	3.9289	0.11	4.0106	-8.2
LacHerbin 18	3.9281	0.12	4.0098	-8.4
LacHerbin 19	3.9272	0.12	4.0089	-8.6
LacHerbin 20	3.9248	0.13	4.0064	-9.2
LacHerbin 21	3.9277	0.11	4.0094	-8.5
			Mean	**-8.5**
			St. dev.	**0.4**
Lamaque Triangle tourmalines from two samples				
85 Lamaque 1	3.8366	0.2	4.0069	-9.1
85 Lamaque 2	3.8252	0.15	3.995	-12,0
85 Lamaque 3	3.8268	0.18	3.9967	-11.6
85 Lamaque 4	3.8285	0.16	3.9985	-11.2
85 Lamaque 5	3.8238	0.16	3.9935	-12.4
85 Lamaque 9	3.8286	0.2	3.9986	-11.1
85 Lamaque 8	3.8294	0.18	3.9994	-10.9
85 Lamaque 7	3.8306	0.24	4.0007	-10.6
85 Lamaque 6	3.8296	0.19	3.9997	-10.9

85 Lamaque 10	3.8325	0.17	4.0026	-10.1
85 Lamaque 11	3.8347	0.18	4.0049	-9.6
			Mean	**-10.8**
			St. dev.	**0.9**
87 Lamaque 1	3.8278	0.17	3.9977	-11.3
87 Lamaque 2	3.8305	0.19	4.0006	-10.6
87 Lamaque 3	3.8307	0.15	4.0007	-10.6
87 Lamaque 4	3.8263	0.16	3.9962	-11.7
87 Lamaque 5	3.8298	0.15	3.9999	-10.8
87 Lamaque 6	3.8284	0.13	3.9984	-11.2
87 Lamaque 7	3.8299	0.27	3.9999	-10.8
87 Lamaque 8	3.8298	0.21	3.9998	-10.8
87 Lamaque 9	3.8293	0.17	3.9993	-11,0
87 Lamaque 10	3.8296	0.17	3.9996	-10.9
			Mean	**-10.9**
			St. dev.	**0.3**
Lamaque Parallel tourmaline from one sample				
88 Lamaque 1	3.823	0.18	3.9928	-12.6
88 Lamaque 2	3.8232	0.19	3.9929	-12.5
88 Lamaque 3	3.8175	0.16	3.987	-14,0
88 Lamaque 4	3.8269	0.22	3.9968	-11.6
88 Lamaque 5	3.8227	0.12	3.9924	-12.7
88 Lamaque 6	3.8234	0.18	3.9932	-12.5
88 Lamaque 7	3.826	0.22	3.9958	-11.8
88 Lamaque 8	3.8229	0.21	3.9926	-12.6
			Mean	**-12.5**
			St. dev.	**0.6**
Goldex tourmalines from one sample				
91 Goldex 1	3.8115	0.16	3.9807	-15.6
91 Goldex 2	3.8141	0.21	3.9834	-14.9
91 Goldex 3	3.8177	0.16	3.9872	-13.9
91 Goldex 4	3.8144	0.15	3.9837	-14.8
91 Goldex 5	3.8135	0.19	3.9828	-15.1
91 Goldex 6	3.8161	0.14	3.9855	-14.4
91 Goldex 8	3.8173	0.14	3.9868	-14.1
91 Goldex 7	3.816	0.17	3.9855	-14.4
			Mean	**-14.6**
			St. dev.	**0.5**

Each analysis is on a different tourmaline grain.
*Internal precision of 20 measurements of $^{11}B/^{10}B$ in ‰ (1 s.d. / mean*1000).
**Corrected for instrument fractionation based on tourmaline reference materials.
*** Values in ‰ relative to NIST SRM 951 (4.04362: Catanzaro *et al*. (1970)).

Appendix : SEM-EDX data from Val-d'Or deposit sample grains.

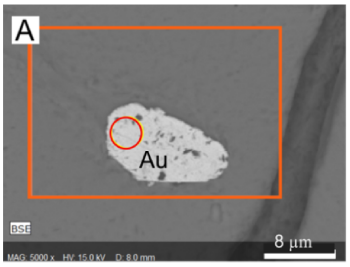

Element	AN	Net	unn. [wt.%]	C norm. [wt.%]	C Atom. [at.%]	C Error [%]
Gold	79	75387	64.52	73.46	38.51	2.4
Sulfur	16	15853	9.98	11.36	36.59	0.4
Iron	26	4146	7.90	9.00	16.64	0.3
Silver	47	3801	4.61	5.25	5.03	0.2
Aluminium	13	1270	0.70	0.79	3.04	0.1
Arsenic	33	128	0.13	0.14	0.20	0.0
Total:		87.83	100.00	100.00		

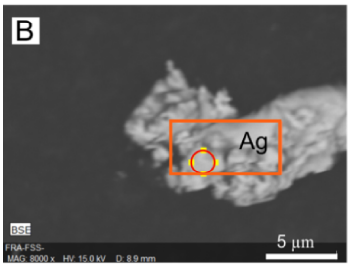

Element	AN	Net	unn. [wt.%]	C norm. [wt.%]	C Atom. [at.%]	C Error [%]
Silver	47	27964	77.55	84.24	38.90	2.4
Carbon	6	3065	10.71	11.63	48.24	1.5
Oxygen	8	327	3.80	4.13	12.86	0.8
Total:		92.06	100.00	100.00		

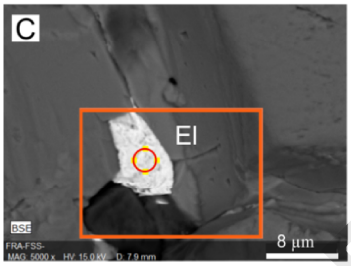

Element	AN	Net	unn. [wt.%]	C norm. [wt.%]	C Atom. [at.%]	C Error [%]
Silver	47	2021	25.45	52.94	32.62	0.8
Sulfur	16	2766	14.27	29.69	61.52	0.5
Gold	79	914	8.35	17.37	5.86	0.3
Total:		48.06	100.00	100.00		

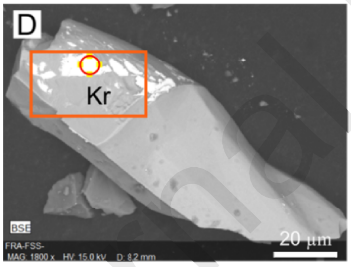

Element	AN	Net	unn. [wt.%]	C norm. [wt.%]	C Atom. [at.%]	C Error [%]
Silver	47	7509	26.98	30.85	13.99	0.9
Tellurium	52	3919	19.24	22.00	8.44	0.6
Gold	79	4331	16.22	18.55	4.61	0.6
Carbon	6	1336	11.89	13.59	55.37	1.9
Iron	26	868	7.14	8.16	7.15	0.2
Sulfur	16	2873	5.98	6.84	10.44	0.2
Total:		87.45	100.00	100.00		

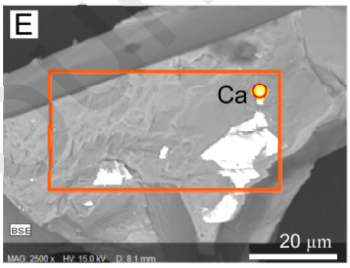

Element	AN	Net	unn. [wt.%]	C norm. [wt.%]	C Atom. [at.%]	C Error [%]
Tellurium	52	2682	33.43	39.02	13.33	1.0
Gold	79	2572	23.08	26.94	5.96	0.9
Carbon	6	499	13.80	16.11	58.45	2.6
Iron	26	326	8.01	9.35	7.30	0.3
Sulfur	16	980	5.28	6.16	8.37	0.2
Oxygen	8	108	2.07	2.42	6.60	0.6
Total:		85.67	100.00	100.00		

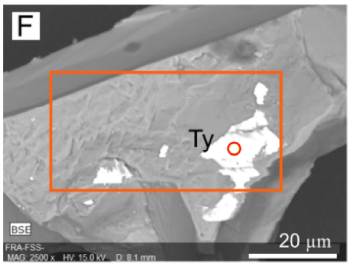

Element	AN	Net	unn. [wt.%]	C norm. [wt.%]	C Atom. [at.%]	C Error [%]
Bismuth	83	3181	32.79	42.16	12.07	1.2
Tellurium	52	2366	26.95	34.65	16.25	0.8
Carbon	6	482	6.68	8.58	42.76	1.3
Iron	26	206	5.48	7.05	7.55	0.2
Oxygen	8	191	3.00	3.86	14.45	0.8
Sulfur	16	584	2.88	3.70	6.9	0.1
Total:		77.78	100.00	100.0		

Highlights –daver et al., 2019

- Geochemistry of pyrite and tourmaline from the Val-d'Or orogenic gold deposit.
- Pyrites record three-stage of formation for the Val-d'Or orogenic gold deposit.
- Gold mineralization occurred during the first of the three stages of deposit formation.
- Tourmaline formation in the veins is related to an oxidized B-bearing supracrustal fluid.
- Tourmaline B-isotope variation is related to deposit proximity to the main or subsidiary fault zones.

Table 1. Mineralogy of the Val-d'Or quartz-carbonate-tourmaline veins.

		Goldex	Lam. Parallel	Lam. Triangle	Lac H.	Beaufor
Pyrite Habit	Cubic Sub-euhedral Anhedral					
Metal inclusions in pyrite or isolated	Gold (Au) Silver (Ag) Electrum (Au,Ag)					
Tellurium	Tellurobismuthite Calaverite ($AuTe_2$) Krennerite (Au_3AgTe_8) Tetradymite (Bi_2Te_2S)					
Tourmaline	Schorl Uvite Dravite					
Barite						
Sulfides	Pyrrhotite (Fe_7S_8) Chalcopyrite ($CuFeS_2$) Molybdenite (MoS)					
	Arsenopyrite (FeAsS)					
Quartz						
Carbonate	Calcite Dolomite					
Feldspar	Albite Microcline (K-feldspar)					
Mica	Biotite Muscovite					
Titanite Scheelite Chlorite Rutile Hematite Apatite						
Zircon						

> 50% of the assemblage

Major mineral in the assemblage

Minor mineral in the assemblage

Table 2. Summary of SIMS B-isotope analyses of select tourmalines.

Analysis	$^{11}B/^{10}B$ (meas.)	int. precision*	$^{11}B/^{10}B$ (corr.)**	$\delta^{11}B$***
Beaufor tourmalines from one sample				
Beaufor 1	3.925	0.13	4.0067	-9.1
Beaufor 2	3.9259	0.1	4.0076	-8.9
Beaufor 3	3.9261	0.1	4.0078	-8.9
Beaufor 4	3.9235	0.12	4.0051	-9.5
Beaufor 5	3.9239	0.12	4.0055	-9.4
Beaufor 6	3.9175	0.12	3.999	-11
Beaufor 7	3.9173	0.16	3.9987	-11.1
Beaufor 8	3.9231	0.1	4.0047	-9.6
Beaufor 9	3.9243	0.11	4.0059	-9.3
Beaufor 10	3.9229	0.09	4.0045	-9.7
Beaufor 11	3.923	0.13	4.0046	-9.6
Beaufor 12	3.924	0.12	4.0056	-9.4
Beaufor 13	3.918	0.15	3.9995	-10.9
Beaufor 14	3.9168	0.15	3.9983	-11.2
Beaufor 15	3.9195	0.15	4.001	-10.5
Beaufor 16	3.9228	0.16	4.0044	-9.7
Beaufor 19 05	3.8293	0.21	3.9993	-10.9
			Mean	**-9.9**
			St. dev.	**0.7**
Lac Herbin tourmalines from one sample				
LacHerbin 1	3.9276	0.1	4.0093	-8.5
LacHerbin 2	3.9294	0.09	4.0112	-8,0
LacHerbin 3	3.9297	0.09	4.0114	-8,0
LacHerbin 4	3.9276	0.1	4.0093	-8.5
LacHerbin 5	3.9243	0.09	4.0059	-9.3
LacHerbin 6	3.9275	0.12	4.0091	-8.5
LacHerbin 7	3.9271	0.14	4.0088	-8.6
LacHerbin 8	3.9272	0.1	4.0089	-8.6
LacHerbin 9	3.9299	0.13	4.0116	-7.9
LacHerbin 10	3.9257	0.13	4.0073	-9,0
LacHerbin 11	3.9307	0.12	4.0125	-7.7
LacHerbin 12	3.9273	0.1	4.0089	-8.6
LacHerbin 13	3.928	0.14	4.0097	-8.4
LacHerbin 14	3.928	0.07	4.0097	-8.4
LacHerbin 15	3.9257	0.13	4.0073	-9,0
LacHerbin 16	3.9265	0.16	4.0082	-8.8
LacHerbin 17	3.9289	0.11	4.0106	-8.2
LacHerbin 18	3.9281	0.12	4.0098	-8.4
LacHerbin 19	3.9272	0.12	4.0089	-8.6
LacHerbin 20	3.9248	0.13	4.0064	-9.2
LacHerbin 21	3.9277	0.11	4.0094	-8.5
			Mean	**-8.5**
			St. dev.	**0.4**
Lamaque Triangle tourmalines from two samples				
85 Lamaque 1	3.8366	0.2	4.0069	-9.1
85 Lamaque 2	3.8252	0.15	3.995	-12,0
85 Lamaque 3	3.8268	0.18	3.9967	-11.6
85 Lamaque 4	3.8285	0.16	3.9985	-11.2
85 Lamaque 5	3.8238	0.16	3.9935	-12.4
85 Lamaque 9	3.8286	0.2	3.9986	-11.1
85 Lamaque 8	3.8294	0.18	3.9994	-10.9
85 Lamaque 7	3.8306	0.24	4.0007	-10.6
85 Lamaque 6	3.8296	0.19	3.9997	-10.9

85 Lamaque 10	3.8325	0.17	4.0026	-10.1
85 Lamaque 11	3.8347	0.18	4.0049	-9.6
			Mean	**-10.8**
			St. dev.	**0.9**
87 Lamaque 1	3.8278	0.17	3.9977	-11.3
87 Lamaque 2	3.8305	0.19	4.0006	-10.6
87 Lamaque 3	3.8307	0.15	4.0007	-10.6
87 Lamaque 4	3.8263	0.16	3.9962	-11.7
87 Lamaque 5	3.8298	0.15	3.9999	-10.8
87 Lamaque 6	3.8284	0.13	3.9984	-11.2
87 Lamaque 7	3.8299	0.27	3.9999	-10.8
87 Lamaque 8	3.8298	0.21	3.9998	-10.8
87 Lamaque 9	3.8293	0.17	3.9993	-11,0
87 Lamaque 10	3.8296	0.17	3.9996	-10.9
			Mean	**-10.9**
			St. dev.	**0.3**
Lamaque Parallel tourmaline from one sample				
88 Lamaque 1	3.823	0.18	3.9928	-12.6
88 Lamaque 2	3.8232	0.19	3.9929	-12.5
88 Lamaque 3	3.8175	0.16	3.987	-14,0
88 Lamaque 4	3.8269	0.22	3.9968	-11.6
88 Lamaque 5	3.8227	0.12	3.9924	-12.7
88 Lamaque 6	3.8234	0.18	3.9932	-12.5
88 Lamaque 7	3.826	0.22	3.9958	-11.8
88 Lamaque 8	3.8229	0.21	3.9926	-12.6
			Mean	**-12.5**
			St. dev.	**0.6**
Goldex tourmalines from one sample				
91 Goldex 1	3.8115	0.16	3.9807	-15.6
91 Goldex 2	3.8141	0.21	3.9834	-14.9
91 Goldex 3	3.8177	0.16	3.9872	-13.9
91 Goldex 4	3.8144	0.15	3.9837	-14.8
91 Goldex 5	3.8135	0.19	3.9828	-15.1
91 Goldex 6	3.8161	0.14	3.9855	-14.4
91 Goldex 8	3.8173	0.14	3.9868	-14.1
91 Goldex 7	3.816	0.17	3.9855	-14.4
			Mean	**-14.6**
			St. dev.	**0.5**

Each analysis is on a different tourmaline grain.
*Internal precision of 20 measurements of $^{11}B/^{10}B$ in ‰ (1 s.d. / mean*1000).
**Corrected for instrument fractionation based on tourmaline reference materials.
*** Values in ‰ relative to NIST SRM 951 (4.04362: Catanzaro *et al*. (1970)).

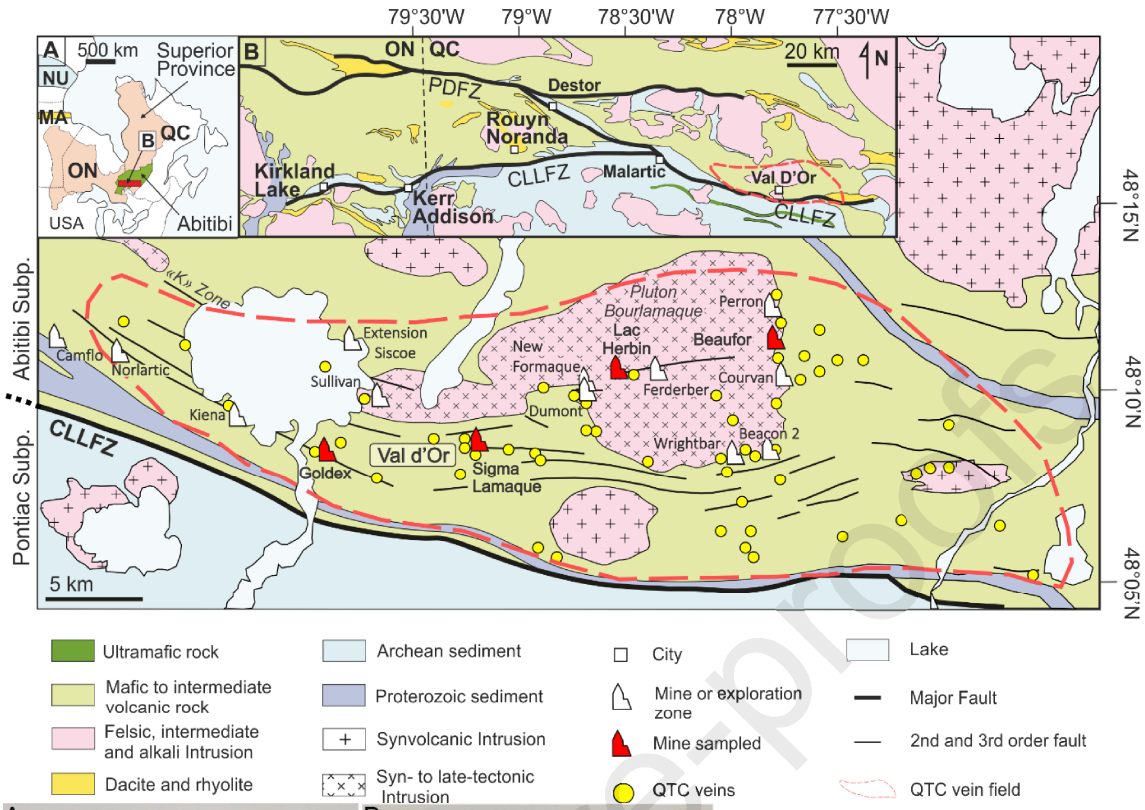
79°30'W
79°W
78°30'W
78°W
77°30'W
A
500 km
Superior Province
NU
MA
ON
QC
B
USA
Abitibi
B
ON
QC
20 km
N
PDFZ
Destor
Rouyn Noranda
Kirkland Lake
Kerr Addison
CLLFZ
Malartic
Val D'Or
CLLFZ
48°15'N
48°10'N
48°05'N
Abitibi Subp.
Pontiac Subp.
«K» Zone
Pluton
Bourlamaque
Perron
Lac Herbin
Beaufor
Extension
Siscoe
Camflo
Norlartic
New Formaque
Courvan
Sullivan
Ferderber
Kiena
Dumont
Beacon 2
Wrightbar
CLLFZ
Val d'Or
Goldex
Sigma
Lamaque
5 km
Ultramafic rock
Mafic to intermediate volcanic rock
Felsic, intermediate and alkali Intrusion
Dacite and rhyolite
Archean sediment
Proterozoic sediment
Synvolcanic Intrusion
Syn- to late-tectonic Intrusion
City
Mine or exploration zone
Mine sampled
QTC veins
Lake
Major Fault
2nd and 3rd order fault
QTC vein field

1

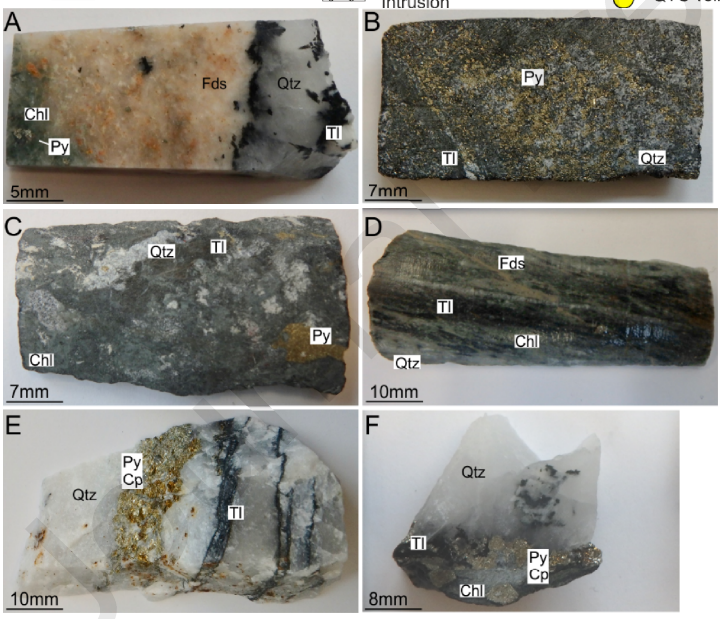
A
Fds
Qtz
Chl
Py
Tl
5mm
B
Py
Tl
Qtz
7mm
C
Qtz
Tl
Py
Chl
7mm
D
Fds
Tl
Chl
Qtz
10mm
E
Py
Cp
Qtz
Tl
10mm
F
Qtz
Tl
Py
Cp
Chl
8mm

2

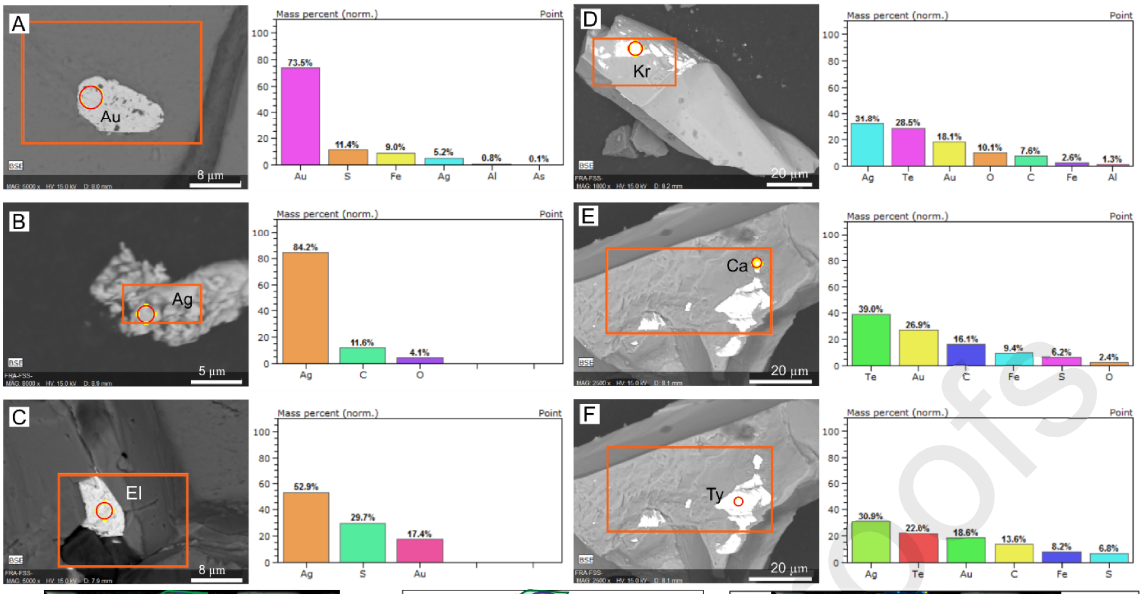
A
Au
8 µm
Mass percent (norm.)
Point
73.5%
11.4%
9.0%
5.2%
0.8%
0.1%
Au
S
Fe
Ag
Al
As
D
Kr
20 µm
31.8%
28.5%
18.1%
10.1%
7.6%
2.6%
1.3%
Ag
Te
Au
O
C
Fe
Al
B
Ag
5 µm
84.2%
11.6%
4.1%
Ag
C
O
E
Ca
20 µm
39.0%
26.9%
16.1%
9.4%
6.2%
2.4%
Te
Au
C
Fe
S
O
C
El
8 µm
52.9%
29.7%
17.4%
Ag
S
Au
F
Ty
20 µm
30.9%
22.6%
18.6%
13.6%
8.2%
6.8%
Ag
Te
Au
C
Fe
S

1

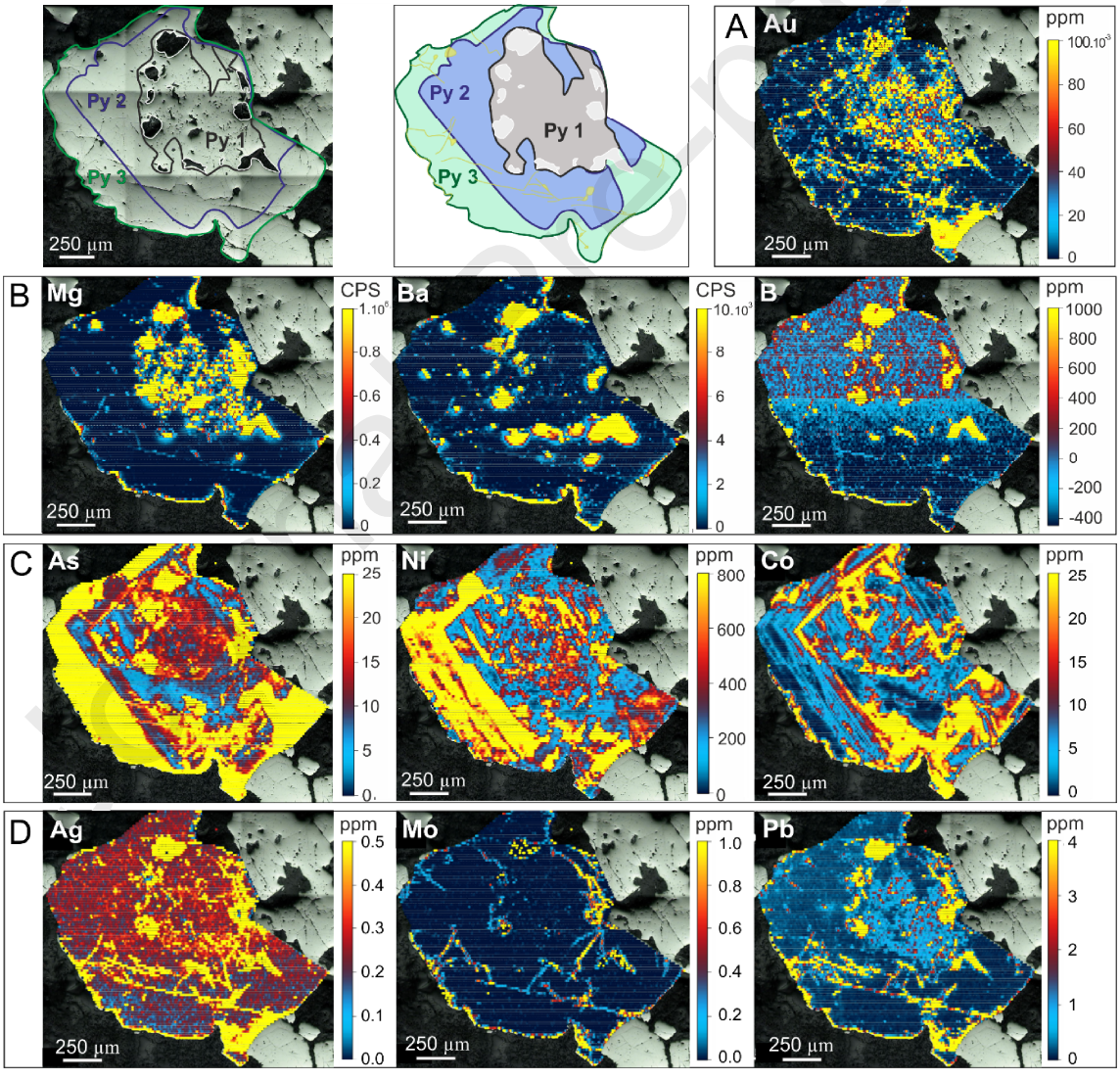
Py 2
Py 1
Py 3
250 µm
A
Au
ppm
100.10⁻³
80
60
40
20
0
B
Mg
CPS
1.10⁶
0.8
0.6
0.4
0.2
0
Ba
CPS
10.10³
8
6
4
2
0
B
ppm
1000
800
600
400
200
0
-200
-400
C
As
ppm
25
20
15
10
5
0
Ni
ppm
800
600
400
200
0
Co
ppm
25
20
15
10
5
0
D
Ag
ppm
0.5
0.4
0.3
0.2
0.1
0.0
Mo
ppm
1.0
0.8
0.6
0.4
0.2
0.0
Pb
ppm
4
3
2
1
0

2

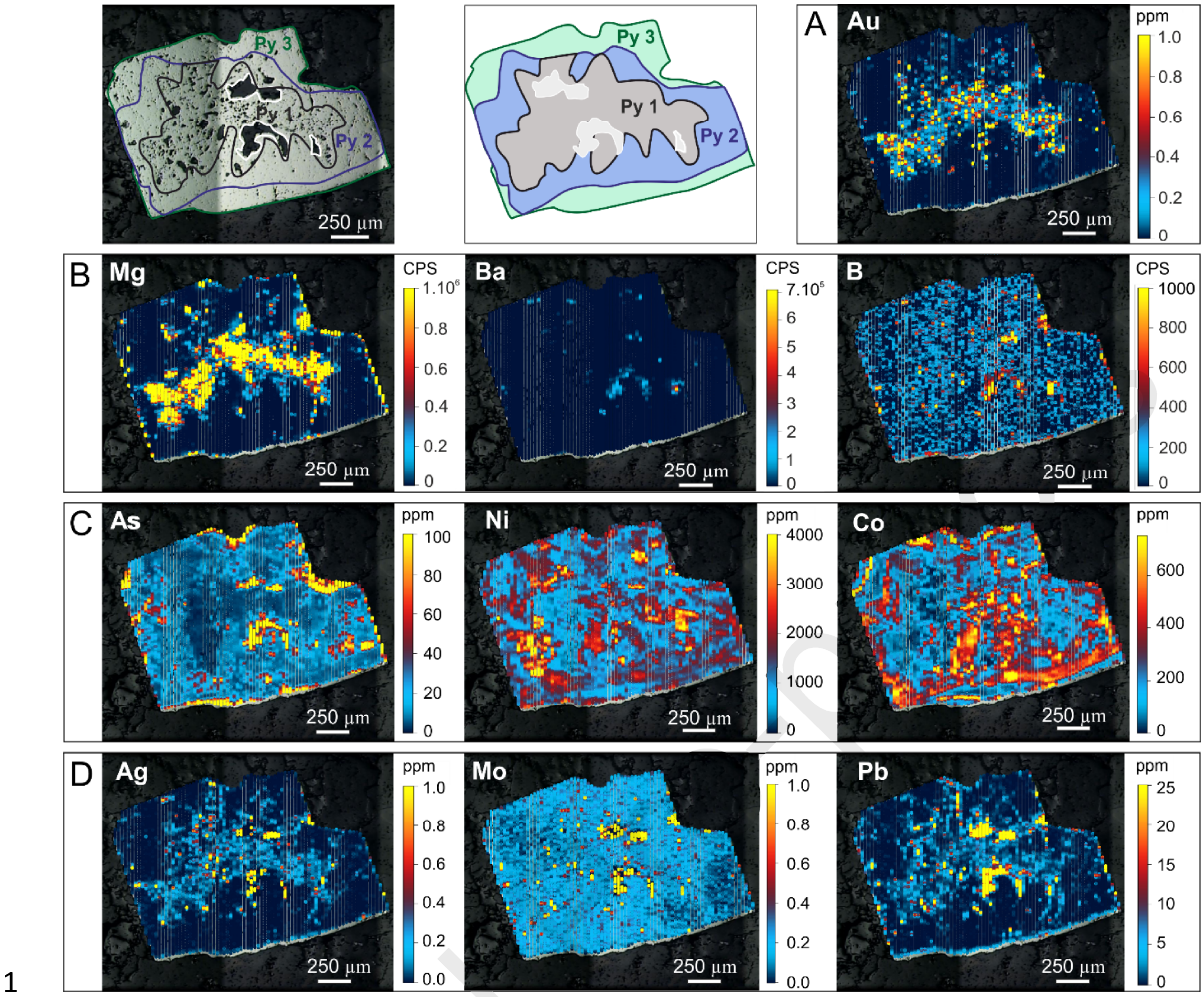
Py 3
Py 1
Py 2
250 µm
A
Au
ppm
1.0
0.8
0.6
0.4
0.2
0
B
Mg
CPS
1.10⁶
Ba
7.10⁶
B
1000
800
600
400
200
C
As
100
80
60
40
20
Ni
4000
3000
2000
1000
Co
D
Ag
Mo
Pb
25
20
15
10
5

1

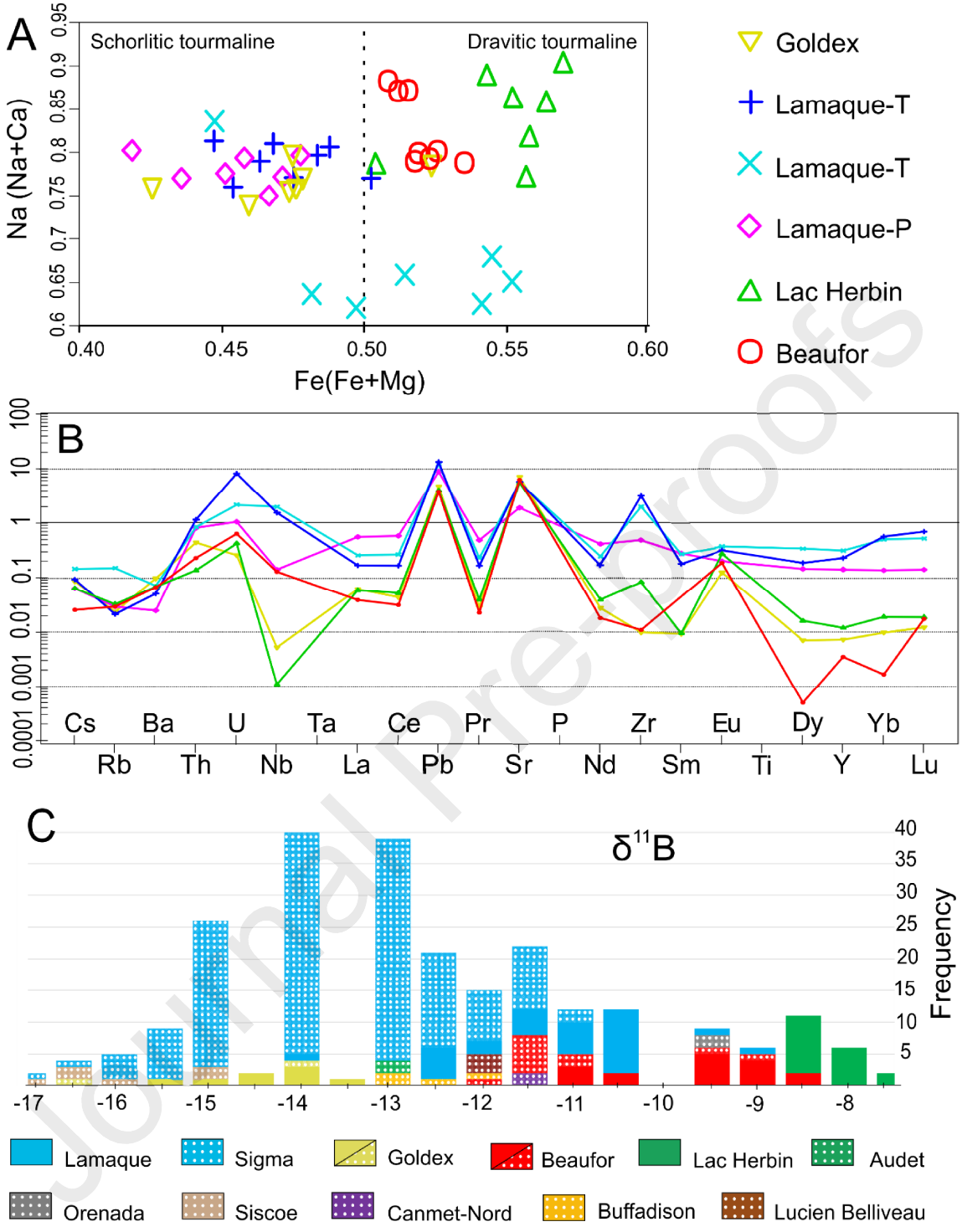

1

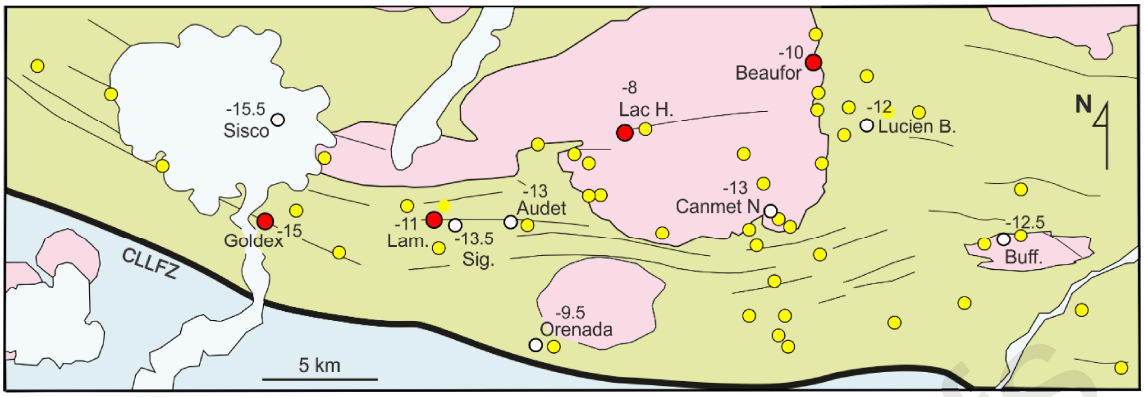

Mafic to intermediate volcanic rock
Felsic, intermediate and alkali intrusion
Archean sediments (Pontiac subprovince)
QTC veins
Mine sampled
Beaudoin et al.
Major Fault CLLFZ
2nd and 3rd order fault
Lake

1

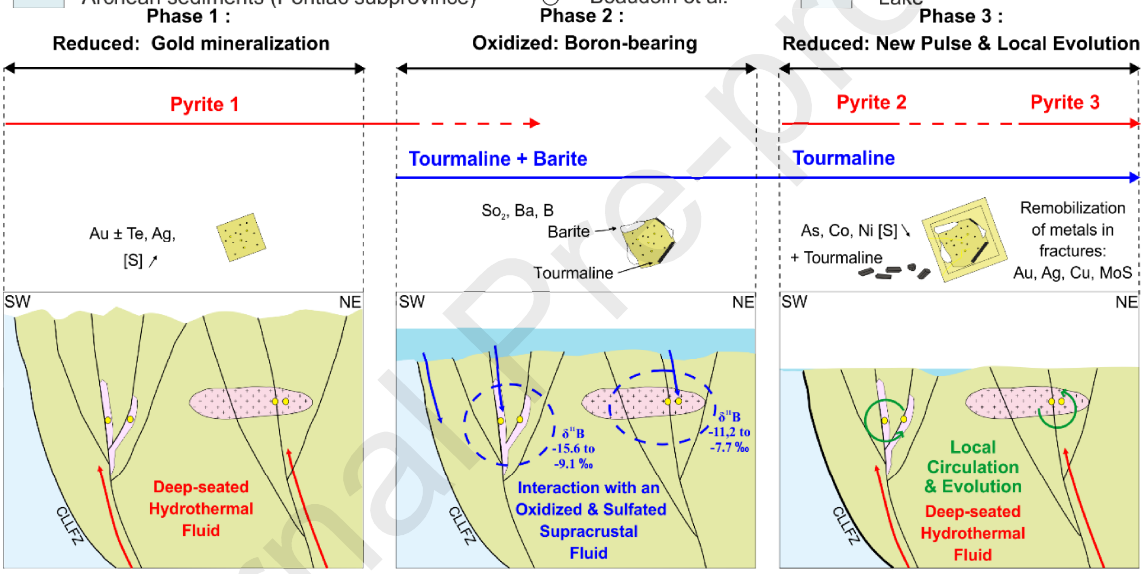

Pontiac Sediments
Archean Seawater
Volcanic Rocks
Input in the fault system
Locale circulation
Local circulation
Bourlamaque Pluton
Dioritic dyke
CLLFZ : Cadillac-Larder Lake Tectonic Fault Zone
Fault
Sample

2

Three-Stage Formation of greenstone-Hosted Orogenic Gold Deposits in the Val-d'Or Mining District, Abitibi, Canada

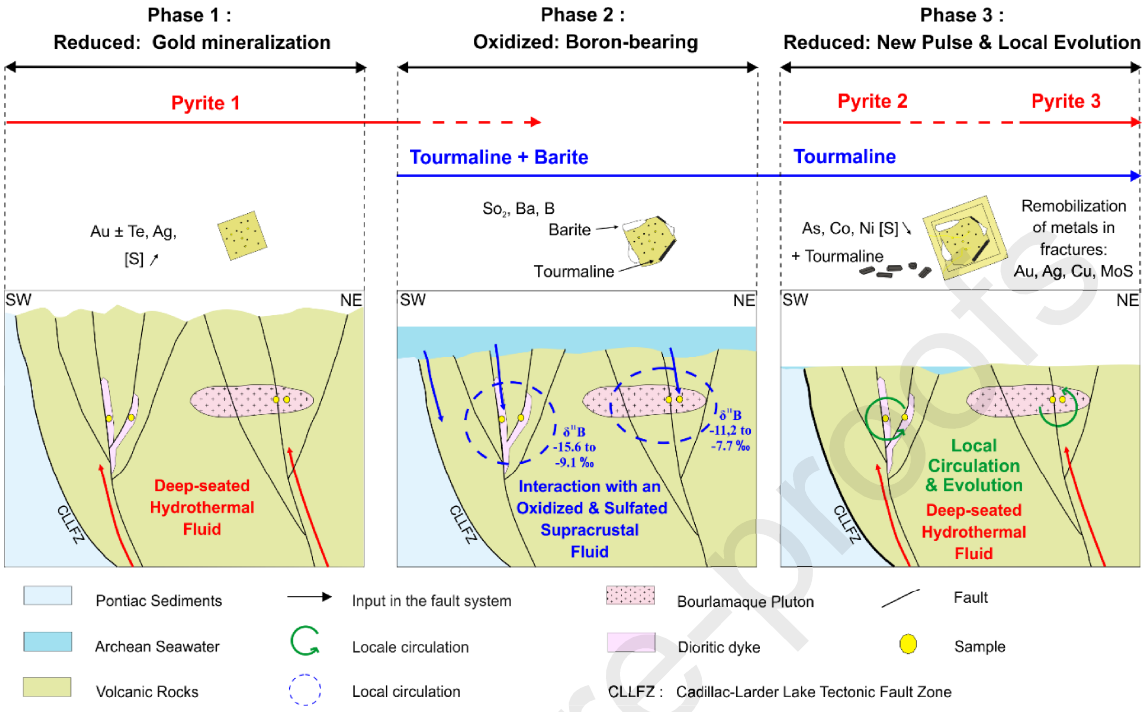

1

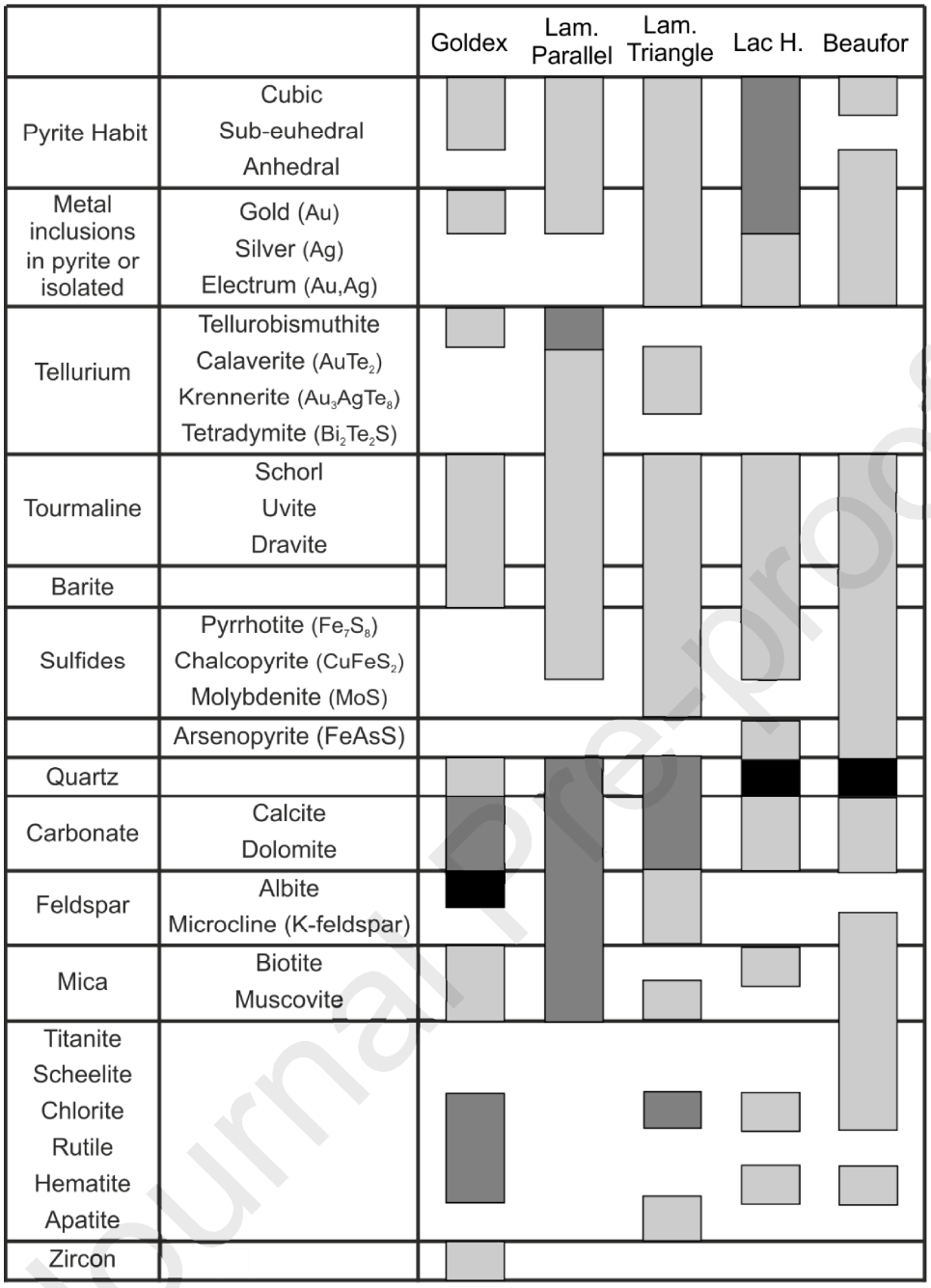

Table A : SEM-EDX data from Val-d'Or deposit sample grains.

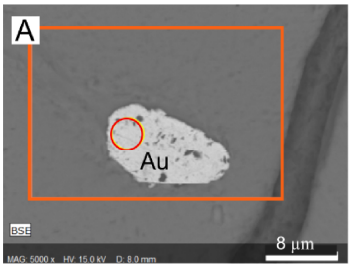

Element	AN	Net	unn. [wt.%]	C norm. [wt.%]	C Atom. [at.%]	C Error [%]
Gold	79	75387	64.52	73.46	38.51	2.4
Sulfur	16	15853	9.98	11.36	36.59	0.4
Iron	26	4146	7.90	9.00	16.64	0.3
Silver	47	3801	4.61	5.25	5.03	0.2
Aluminium	13	1270	0.70	0.79	3.04	0.1
Arsenic	33	128	0.13	0.14	0.20	0.0
Total:			87.83	100.00	100.00	

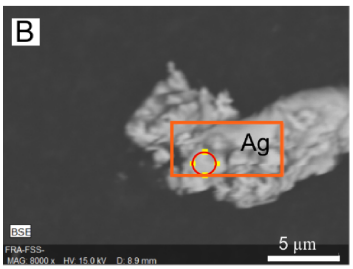

Element	AN	Net	unn. [wt.%]	C norm. [wt.%]	C Atom. [at.%]	C Error [%]
Silver	47	27964	77.55	84.24	38.90	2.4
Carbon	6	3065	10.71	11.63	48.24	1.5
Oxygen	8	327	3.80	4.13	12.86	0.8
Total:			92.06	100.00	100.00	

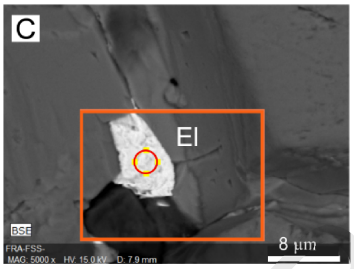

Element	AN	Net	unn. [wt.%]	C norm. [wt.%]	C Atom. [at.%]	C Error [%]
Silver	47	2021	25.45	52.94	32.62	0.8
Sulfur	16	2766	14.27	29.69	61.52	0.5
Gold	79	914	8.35	17.37	5.86	0.3
Total:			48.06	100.00	100.00	

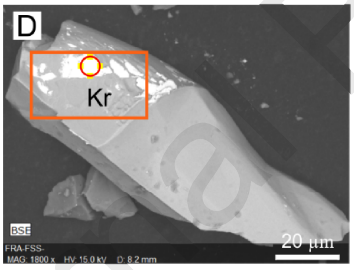

Element	AN	Net	unn. [wt.%]	C norm. [wt.%]	C Atom. [at.%]	C Error [%]
Silver	47	7509	26.98	30.85	13.99	0.9
Tellurium	52	3919	19.24	22.00	8.44	0.6
Gold	79	4331	16.22	18.55	4.61	0.6
Carbon	6	1336	11.89	13.59	55.37	1.9
Iron	26	868	7.14	8.16	7.15	0.2
Sulfur	16	2873	5.98	6.84	10.44	0.2
Total:			87.45	100.00	100.00	

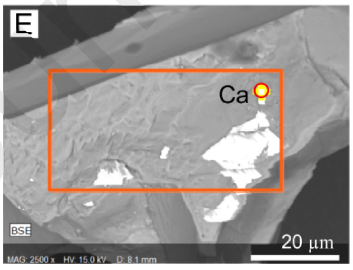

Element	AN	Net	unn. [wt.%]	C norm. [wt.%]	C Atom. [at.%]	C Error [%]
Tellurium	52	2682	33.43	39.02	13.33	1.0
Gold	79	2572	23.08	26.94	5.96	0.9
Carbon	6	499	13.80	16.11	58.45	2.6
Iron	26	326	8.01	9.35	7.30	0.3
Sulfur	16	980	5.28	6.16	8.37	0.2
Oxygen	8	108	2.07	2.42	6.60	0.6
Total:			85.67	100.00	100.00	

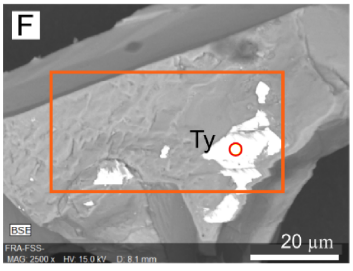

Element	AN	Net	unn. [wt.%]	C norm. [wt.%]	C Atom. [at.%]	C Error [%]
Bismuth	83	3181	32.79	42.16	12.07	1.2
Tellurium	52	2366	26.95	34.65	16.25	0.8
Carbon	6	482	6.68	8.58	42.76	1.3
Iron	26	206	5.48	7.05	7.55	0.2
Oxygen	8	191	3.00	3.86	14.45	0.8
Sulfur	16	584	2.88	3.70	6.9	0.1
Total:			77.78	100.00	100.0	

1

Appendix

Table B: LA-ICP-MS analyses for major, trace and rare earth elements of selected tourmaline samples from Val-d'Or . Si=6 and O=29

		Oxide														Major elements									
		SiO2	TiO2	Al2O3	FeO	MgO	MnO	CaO	Na2O	K2O	Li2O	Cr2O3	B2O3	H2O	ZnO	Si	Na	Ca	Mg	Fe	Al	K	Ti	Cr	Mn
							x10^{-3}			x10^{-3}	x10^{-3}	x10^{-3}				x10^{4}					x10^{4}				
Mine	Sample	%wt														ppm									
Goldex	TL-91-1	35,11	0,33	34,42	5,48	7,84	6,30	0,76	2,26	8,30	0,40	128,10	10,17	3,51	15,30	16,98	17336,58	5603,4	48902,4	44046,1	18,8	71,3	2024,0	906,7	50,2
	TL-91-2	35,92	0,49	34,07	4,65	8,09	7,00	0,69	2,09	5,00	0,50	0,20	10,40	3,59	13,50	16,98	15655,56	4958,2	49360,9	36574,9	18,2	42,2	2968,1	1,7	55,2
	TL-91-3	36,28	0,27	34,32	5,04	7,18	5,10	0,58	2,19	8,30	0,50	8,90	10,51	3,63	18,80	16,98	16266,84	4126,1	43349,9	39206,8	18,2	69,1	1604,6	61,3	39,4
	TL-91-4	35,13	0,33	35,87	5,60	6,55	5,20	0,60	2,11	8,10	0,40	98,10	10,18	3,51	20,20	16,98	16181,94	4408,0	40870,9	45031,0	19,6	69,6	2069,9	693,8	41,3
	TL-91-5	35,69	0,37	34,01	5,14	7,79	7,80	0,80	2,19	6,50	0,20	95,60	10,34	3,57	12,80	16,98	16538,52	5807,2	47798,7	40650,1	18,3	55,2	2248,2	665,6	61,3
	TL-91-6	36,20	0,35	33,38	5,32	7,55	7,90	0,75	2,26	7,90	0,20	74,90	10,49	3,62	11,20	16,98	16861,14	5360,6	45676,2	41516,1	17,7	65,7	2091,9	514,5	61,6
	TL-91-7	36,22	0,32	33,24	5,38	7,56	7,70	0,71	2,30	8,50	0,30	135,30	10,49	3,62	11,50	16,98	17132,82	5094,0	45710,2	41974,6	17,6	71,2	1912,0	928,8	59,6
	TL-91-8	35,97	0,29	34,85	4,65	7,39	5,70	0,62	2,19	9,70	0,40	25,30	10,42	3,59	18,60	16,98	16385,7	4465,7	44997,0	36507,0	18,6	81,5	1742,2	174,9	44,8
Lamaque																									
Parallel	TL-88-1	33,86	0,23	38,64	4,48	7,01	25,70	0,58	1,94	4,60	1,00	30,80	9,81	3,38	15,40	16,98	15451,8	4465,7	45353,6	37322,0	21,9	41,1	1468,8	225,8	213,8
	TL-88-2	34,94	0,48	37,37	4,42	6,74	24,40	0,51	1,89	4,60	0,90	2,50	10,12	3,49	14,80	16,98	14585,8	3788,2	42246,2	35691,9	20,6	39,4	3005,5	17,7	196,8
	TL-88-3	34,82	0,23	37,46	4,77	6,72	26,10	0,50	1,90	4,90	1,20	1,50	10,09	3,48	17,20	16,98	14738,64	3744,1	42263,2	38663,5	20,7	42,5	1419,5	10,4	210,9
	TL-88-4	35,43	0,20	36,80	4,09	7,33	24,50	0,47	1,83	4,00	0,90	18,10	10,26	3,54	9,30	16,98	13940,58	3430,0	45336,6	32601,6	20,0	34,3	1234,4	126,7	194,3
	TL-88-5	34,24	0,18	39,13	4,06	6,77	26,20	0,51	1,65	4,00	1,10	105,70	9,92	3,42	4,70	16,98	12972,72	3854,5	43299,0	33450,6	22,0	35,3	1159,7	767,5	215,5
	TL-88-6	33,82	0,26	37,07	4,60	6,74	25,20	2,43	1,87	3,50	1,20	1,20	9,80	3,38	13,60	16,98	14891,4	18678,0	43638,6	38374,8	21,1	31,0	1653,9	9,0	209,9
	TL-88-7	35,68	0,31	36,33	4,55	6,58	24,30	0,61	2,00	4,20	1,00	1,10	10,34	3,57	14,60	16,98	15078,24	4448,8	40395,4	36031,6	19,6	35,1	1900,1	7,8	191,5
	TL-88-8	34,54	0,64	36,85	4,88	7,19	47,90	0,61	1,76	4,90	0,60	21,20	10,00	3,45	10,10	16,98	13736,82	4572,7	45625,3	39903,0	20,5	43,1	4041,2	152,8	390,5
Triangle	TL-87-1	34,06	2,87	33,96	6,21	6,48	27,50	1,11	1,99	6,50	1,90	9,90	9,87	3,40	11,20	16,98	15774,42	8456,0	41702,9	51449,4	19,2	57,4	18338,4	72,2	227,5
	TL-87-2	34,54	3,72	33,40	5,50	6,69	24,20	0,93	1,73	5,90	1,90	3,70	10,00	3,45	10,00	16,98	13482,12	6978,8	42450,0	44997,0	18,6	51,4	23432,4	26,3	197,0
	TL-87-3	38,34	1,58	30,92	5,33	5,82	26,60	1,16	1,86	10,30	1,90	12,70	11,11	3,83	11,10	16,98	13091,58	7844,8	33229,9	39240,8	15,5	80,7	8948,5	82,0	195,3
	TL-87-4	34,86	2,81	33,22	6,22	6,69	21,40	0,84	1,73	15,90	2,50	11,10	10,10	3,48	11,20	16,98	13346,2	6282,6	42008,5	50345,7	18,3	137,5	17557,3	79,0	173,0
	TL-87-5	33,65	1,68	36,80	5,08	7,04	16,60	0,97	1,63	10,00	2,00	6,70	9,75	3,36	6,90	16,98	13074,6	7471,2	45846,0	42619,8	21,0	90,0	10867,2	49,2	138,9
	TL-87-6	37,13	0,36	35,02	3,71	5,90	20,80	0,57	2,81	4,90	1,20	12,80	10,76	3,71	11,60	16,98	20376	3990,3	34809,0	28186,8	18,1	39,7	2105,5	85,4	157,9
	TL-87-7	30,96	2,63	33,91	6,50	6,47	112,10	5,53	1,79	4,60	1,90	21,50	8,97	3,09	17,80	16,98	15621,6	46355,4	45778,1	59260,2	21,1	44,7	18508,2	172,7	1018,8
	TL-87-8	36,50	0,53	33,47	5,05	6,58	24,00	1,40	2,20	14,10	1,70	7,90	10,57	3,65	7,30	16,98	16249,86	9933,3	39478,5	39054,0	17,6	116,7	3173,6	53,5	185,1
	TL-85-1	35,45	0,48	35,22	5,14	7,07	11,30	0,59	2,22	7,40	1,70	13,00	10,27	3,54	48,70	16,98	16861,14	4287,5	43672,6	40938,8	19,1	63,0	2920,6	91,4	90,0
	TL-85-2	34,28	0,36	37,24	5,32	6,78	11,80	0,62	2,02	6,90	1,80	1,10	9,93	3,43	51,60	16,98	15876,3	4720,4	43333,0	43791,4	20,9	60,5	2268,5	7,8	97,1
	TL-85-3	35,91	0,38	34,95	4,78	7,12	10,20	0,61	2,23	6,60	2,10	1,30	10,40	3,59	59,60	16,98	16708,32	4438,6	43451,8	37576,7	18,7	55,1	2321,2	9,3	79,8
	TL-85-4	33,02	3,97	35,52	5,01	6,77	10,50	0,55	2,21	5,90	2,00	74,70	9,56	3,30	68,50	16,98	18066,72	4341,8	44929,1	42823,6	20,7	54,3	26149,2	562,0	89,7
	TL-85-5	34,13	0,46	37,26	4,83	7,07	10,10	0,55	2,25	6,00	1,80	134,30	9,89	3,41	63,60	16,98	17761,08	4153,3	45370,6	39987,9	21,0	53,3	2954,5	978,1	83,4
	TL-85-6	35,28	0,83	35,93	4,48	7,14	11,90	0,50	2,09	5,40	1,90	2,30	10,22	3,53	57,10	16,98	15927,24	3650,7	44317,8	35878,7	19,6	46,5	5094,0	16,0	94,6
	TL-85-7	35,38	0,44	35,74	4,94	7,02	11,00	0,63	2,04	6,10	2,00	20,30	10,25	3,54	43,60	16,98	15553,68	4601,6	43468,8	39393,6	19,4	52,3	2679,4	142,6	87,5
	TL-85-8	34,47	2,37	35,13	4,60	7,13	12,30	0,69	2,10	5,60	1,90	53,00	9,99	3,45	66,60	16,98	16436,64	5178,9	45336,6	37695,6	19,6	49,4	14942,4	382,1	100,5
Lac Herbin	TL-73-1	34,69	0,41	35,36	6,40	6,56	14,20	0,71	2,31	13,00	1,30	0,40	10,05	3,47	12,80	16,98	17964,84	5314,7	41431,2	52128,6	19,6	113,4	2597,9	2,7	115,3
	TL-73-2	33,25	0,28	37,85	5,72	7,24	12,20	0,59	2,09	10,20	1,30	1,50	9,63	3,32	7,20	16,98	16980	4601,6	47713,8	48562,8	21,9	92,7	1813,5	10,9	103,4
	TL-73-3	33,61	0,11	37,64	6,23	6,74	12,60	0,29	2,26	8,00	1,30	2,40	9,74	3,36	13,40	16,98	18134,64	2265,1	43927,3	52298,4	21,5	71,8	680,9	18,0	105,6
	TL-73-4	35,73	0,30	34,78	6,12	6,25	11,80	0,54	2,34	11,00	1,10	1,40	10,35	3,57	11,80	16,98	17642,22	3922,4	38289,9	48393,0	18,7	92,5	1805,0	9,8	92,5
	TL-73-5	36,69	0,17	34,83	5,94	5,78	5,00	0,23	2,04	5,90	1,30	16,60	10,63	3,67	12,40	16,98	14976,36	1602,9	34486,4	45744,1	18,3	48,7	1015,4	112,7	38,7
	TL-73-6	34,59	0,22	36,17	6,43	6,39	12,30	0,39	2,30	9,40	1,10	2,50	10,02	3,46	14,20	16,98	17913,9	2957,9	40480,3	52468,2	20,1	81,8	1358,4	17,8	99,8
	TL-73-7	35,09	0,25	35,58	6,05	6,31	6,30	0,36	2,20	7,50	1,20	477,00	10,17	3,51	12,00	16,98	16895,1	2682,8	39376,6	48647,7	19,5	64,4	1558,8	3379,0	50,6
Beaufor	TL-10-1	34,90	0,65	34,22	6,24	7,33	14,10	0,65	2,39	12,90	0,80	1,80	10,11	3,49	7,40	16,98	18440,28	4798,5	45998,8	50481,5	18,8	111,0	4075,2	12,6	113,4
	TL-10-2	35,06	0,48	34,59	6,06	7,23	14,20	0,59	2,28	15,90	0,70	5,50	10,16	3,50	6,90	16,98	17523,36	4387,6	45166,8	48800,5	19,0	136,9	3003,8	39,2	113,6
	TL-10-3	34,83	0,52	34,70	6,09	7,29	13,60	0,64	2,33	13,10	0,70	1,90	10,09	3,48	7,70	16,98	18015,78	4788,4	45863,0	49343,9	19,2	113,4	3243,2	13,8	109,7
	TL-10-4	35,34	0,13	35,48	5,69	7,09	10,90	0,30	2,18	8,40	0,70	17,80	10,24	3,53	11,40	16,98	16589,46	2190,4	43927,3	45438,5	19,3	71,3	789,6	125,5	86,9
	TL-10-5	34,64	0,17	36,34	5,73	7,03	15,80	0,34	2,22	11,70	0,70	3,10	10,03	3,46	9,10	16,98	17251,68	2550,4	44487,6	46695,0	20,2	101,7	1095,2	22,2	128,7
	TL-10-6	34,71	0,46	35,35	6,14	6,86	14,20	0,64	2,28	14,60	0,90	5,00	10,06	3,47	10,90	16,98	17693,16	4754,4	43299,0	49921,2	19,6	126,8	2901,9	36,0	114,8
	TL-10-7	34,80	0,20	36,57	5,63	6,81	12,10	0,32	2,09	8,00	0,80	1,00	10,08	3,48	10,40	16,98	16181,94	2370,4	42874,5	45676,2	20,2	68,9	1282,0	7,1	97,8
	TL-10-8	34,00	0,50	35,94	6,17	7,17	12,60	0,60	2,34	12,00	0,80	11,50	9,85	3,40	8,80	16,98	18576,12	4601,6	46185,6	51279,6	20,3	106,8	3175,3	84,2	104,1

Mine	Sample	Trace element Co	Li	Be	Sc	Ni	Cu	V	Zn	Ga	Rb x10^{-2}	Sr	Y	Zr	Nb	Mo	Ag	Cd	In	Sn	Sb	Cs x10^{-3}	Ba	Hf x10^{-3}	W	Au	Tl x10^{-3}	Pb	Bi x10^{-3}	Th x10^{-3}	U x10^{-3}
		ppm																													
Goldex	TL-91-1	0,37	1,78	0,00	45,08	177,95	3,14	456,76	122,77	57,39	3,4	784,48	0,00	0,11	0,00	0,000	0,085	0,082	0,071	0,885	0,048	2,5	2,61	0	0,00	0	2,7	3,84	83,2	0	0,1
	TL-91-2	1,06	2,14	0,21	28,34	194,25	1,95	448,27	108,16	43,83	2,78	443,18	0,01	0,01	0,00	0,000	0,058	0,158	0,033	0,406	0,022	0	0,56	0	0,02	0	6,1	2,22	63,3	3,9	0,2
	TL-91-3	0,70	2,47	0,44	24,76	107,99	2,04	450,82	151,29	51,40	4,25	735,23	0,03	0,06	0,02	0,037	0,061	0,095	0,050	0,696	0,051	6,3	1,19	0	0,02	0,0815	8,2	3,58	90	781,1	90
	TL-91-4	1,24	1,85	4,13	56,37	141,61	3,97	641,67	162,67	58,75	3,51	998,42	0,25	0,11	0,01	0,000	0,032	0,195	0,092	0,735	0,166	9	1,51	7,3	0,11	0,0679	2,2	4,58	60,8	28,9	7,5
	TL-91-5	0,40	1,15	0,24	52,98	140,59	1,97	449,46	102,73	51,14	2,39	714,86	0,07	0,03	0,01	0,000	0,027	0,117	0,078	0,808	0,066	2,2	1,95	0	0,03	0,0068	7,8	2,90	59,3	10,2	0,2
	TL-91-6	1,03	1,15	0,07	37,08	144,67	2,36	442,67	89,82	47,90	2,05	745,42	0,04	0,09	0,01	0,000	0,059	0,051	0,052	0,791	0,053	8,3	2,26	0	0,03	0,0204	4,6	3,21	42,1	90	13,4
	TL-91-7	0,64	1,29	0,07	37,42	145,01	5,84	475,44	92,03	52,13	3,74	653,73	0,10	1,17	0,01	0,029	0,078	0,019	0,076	0,931	0,095	13,1	2,94	6,1	0,05	0	13,4	2,99	61,1	12,9	20,4
	TL-91-8	0,28	1,77	0,34	39,05	91,69	3,74	436,39	149,76	56,20	5,09	794,66	0,03	0,19	0,00	0,000	0,043	0,061	0,063	0,849	0,037	0	1,88	6,5	0,02	0,0441	12,2	4,50	91,7	84,9	6,8
Lamaque																															
Parallel	TL-88-1	0,67	5,16	1,24	22,14	17,10	2,75	251,98	123,44	40,23	2,6	182,87	1,66	0,09	0,00	0,000	0,053	0,311	0,109	1,754	0,037	9,5	0,00	0	0,01	0,0425	12,1	5,89	146	764,1	23,8
	TL-88-2	0,61	4,25	1,61	17,47	17,29	2,45	245,70	118,52	38,00	3,06	175,91	0,15	3,06	2,14	0,000	0,034	0,149	0,117	2,292	0,109	3,2	0,09	69,6	2,46	0,0187	8,7	5,21	122,3	25,5	8
	TL-88-3	0,82	5,93	1,14	11,21	25,47	2,46	232,63	137,88	37,19	2,63	178,29	0,23	0,28	0,00	0,000	0,073	0,206	0,060	1,552	0,053	6,8	0,20	0	0,01	0,0187	3,6	5,21	88,5	17,1	7,8
	TL-88-4	0,61	4,26	1,21	30,67	13,92	6,64	199,85	74,71	32,77	10,19	141,27	0,17	1,32	0,01	0,153	0,071	0,255	0,090	1,885	0,146	7,3	0,83	4,4	0,05	0,1749	10,7	22,24	322,6	237,7	164,7
	TL-88-5	1,07	5,33	0,83	15,62	36,51	14,79	201,72	37,70	33,96	3,74	178,29	0,37	2,89	0,00	0,000	0,204	0,000	0,086	1,953	0,122	0	0,66	59,4	0,03	0,1409	17	3,72	217,3	26,1	22,1
	TL-88-6	1,05	5,94	0,08	20,19	20,04	4,69	255,72	109,18	38,71	3,57	118,01	11,89	137,54	0,03	0,577	0,061	0,241	0,136	2,751	0,039	0	0,53	4075,2	0,18	0,0306	1,5	4,16	157,9	933,9	424,5
	TL-88-7	1,03	4,82	1,77	20,27	16,90	3,45	274,91	117,33	41,26	3,06	137,88	0,38	2,39	0,06	0,019	0,026	0,024	0,129	2,411	0,037	1,2	0,11	69,6	0,10	0,0119	9	4,33	47,9	17	16,1
	TL-88-8	1,29	3,07	6,23	23,26	21,73	15,79	244,34	81,33	34,52	5,77	210,38	0,10	2,04	0,02	0,132	0,139	0,041	0,117	2,460	0,100	1,2	0,75	52,6	0,06	0,0543	7,3	6,20	346,4	5,3	9
Triangle	TL-87-1	19,31	9,25	7,86	40,07	71,66	4,33	740,33	89,82	23,64	13,07	665,62	4,41	69,62	6,96	0,000	0,083	0,124	0,022	0,798	1,358	6,8	0,71	1935,7	39,22	-0,0068	19,2	11,80	198,7	180	210,6
	TL-87-2	27,34	9,22	0,87	32,43	31,07	6,49	736,93	80,66	25,25	12,4	514,49	1,87	88,47	12,74	0,000	0,117	0,121	0,032	1,274	1,681	0	0,49	3073,4	50,60	0,0509	12,1	10,77	220,7	140,9	259,8
	TL-87-3	23,69	8,22	4,86	32,75	36,17	3,04	607,37	89,31	18,80	31,07	516,53	0,76	10,88	3,11	0,058	0,073	0,679	0,023	0,469	0,662	19,2	1,22	312,4	16,98	0,0645	7,3	9,34	171,5	91,7	63,2
	TL-87-4	23,35	11,99	5,09	34,54	33,79	4,84	669,01	90,33	22,19	55,69	640,15	5,62	264,89	8,42	0,000	0,136	0,136	0,030	1,335	1,031	21,4	1,72	8065,5	42,28	0,0221	16	11,31	222,4	385,4	436,4
	TL-87-5	36,17	10,26	0,63	29,63	41,43	6,01	594,30	55,35	22,86	39,39	480,53	10,87	99,50	4,70	0,000	0,117	0,088	0,040	0,897	0,611	7,3	2,33	2665,9	17,66	0,0475	16,1	9,51	239,4	76,4	113,8
	TL-87-6	0,35	5,45	0,29	14,13	11,04	4,13	163,17	93,56	30,56	16,3	110,20	4,25	0,68	1,95	0,058	0,117	0,172	0,066	1,562	0,053	10,4	1,27	45,8	2,22	0,073	14,1	4,08	171,5	730,1	54,3
	TL-87-7	33,45	10,36	1,36	53,66	55,52	4,04	809,95	143,14	29,36	10,19	708,07	8,73	202,06	7,95	0,041	0,148	0,730	0,065	1,038	1,970	8,3	0,66	5569,4	46,86	0,0425	14,1	12,72	178,3	497,5	377
	TL-87-8	28,78	7,78	4,47	31,07	33,28	4,58	601,09	58,92	21,28	44,15	772,59	0,29	5,04	0,14	0,000	0,132	0,014	0,027	0,521	0,083	1,7	2,04	129	0,41	0,0526	2,2	13,70	156,2	13,8	18,2
	TL-85-1	1,90	8,01	0,95	50,43	25,81	4,91	469,33	391,39	39,12	2,56	621,47	2,58	159,61	0,47	0,017	0,216	0,105	0,051	0,654	0,216	0	0,39	4686,5	4,77	0,1223	4,4	11,89	230,9	259,8	541,7
	TL-85-2	4,94	8,95	0,73	59,77	43,30	3,09	437,07	414,48	35,73	3,19	619,77	0,02	0,19	0,00	0,000	0,066	0,112	0,047	0,363	0,082	5,3	0,41	0	0,01	0,034	5,4	7,22	137,5	0	0
	TL-85-3	0,58	9,97	0,78	75,73	17,18	4,02	504,82	478,84	42,08	3,77	584,79	0,67	24,11	0,05	0,036	0,054	0,328	0,046	0,679	0,178	9,3	1,39	650,3	0,58	0	7	10,88	93,1	81,5	107
	TL-85-4	1,12	10,10	0,92	88,98	16,30	5,96	618,07	550,15	45,00	2,05	584,11	10,53	579,02	20,72	0,053	0,238	0,445	0,062	2,292	3,719	10,7	1,41	16844,2	146,03	0,0204	8	14,72	154,5	1511,2	3022,4
	TL-85-5	1,38	9,12	0,46	63,34	20,65	4,31	474,25	511,10	41,31	3,4	592,60	3,07	146,03	0,62	0,054	0,116	0,391	0,026	0,399	0,180	7,5	0,63	4516,7	4,55	0	12,4	11,68	215,6	341,3	823,5
	TL-85-6	1,26	9,08	0,71	60,96	16,93	5,14	477,14	458,46	41,26	3,57	421,10	3,09	149,42	2,63	0,000	0,083	0,160	0,044	0,815	0,584	0	0,62	3446,9	20,72	0,0272	11,7	8,95	213,9	288,7	631,7
	TL-85-7	1,90	9,41	0,65	41,94	37,70	4,60	438,08	350,30	38,05	2,38	599,39	0,48	31,41	0,12	0,000	0,093	0,151	0,034	0,530	0,112	0	0,19	849	1,21	0,0323	6,8	10,41	356,6	56	163
	TL-85-8	0,91	9,46	0,68	101,03	17,66	4,58	565,43	534,87	45,51	3,57	616,37	5,55	139,24	10,02	0,000	0,117	0,340	0,056	1,545	1,375	12,6	2,14	4075,2	73,01	0	9,2	14,65	84,9	453,4	1647,1
Lac Herbin	TL-73-1	16,56	6,27	2,12	33,79	42,96	6,62	461,86	102,73	38,88	6,45	908,43	0,07	0,42	0,01	0,027	0,066	0,543	0,104	1,715	0,061	6,3	0,98	8,5	0,05	0,0441	12,2	5,09	217,3	39,1	9,5
	TL-73-2	15,98	6,38	0,53	42,45	50,43	5,08	410,92	57,56	39,56	4,58	964,46	0,06	1,53	0,00	0,000	0,459	0,238	0,100	1,613	0,119	0	1,31	23,8	0,00	0,1223	10,4	4,14	450	16,3	22,1
	TL-73-3	23,81	6,28	0,46	97,47	66,39	3,48	409,05	107,82	42,08	5,09	316,51	0,00	0,09	0,00	0,000	0,031	0,207	0,146	2,785	0,017	3,2	0,31	0	0,00	0	4,2	1,90	163	6,1	0
	TL-73-4	15,55	4,99	0,58	58,58	60,96	3,36	482,57	94,75	43,30	4,08	684,29	0,00	0,06	0,00	0,000	0,039	0,109	0,116	2,284	0,107	0	1,43	0	0,05	0	3,6	2,57	168,1	11,9	7,3
	TL-73-5	16,95	6,11	1,09	30,28	343,85	4,02	496,33	99,33	32,50	4,23	261,32	0,25	0,22	0,00	0,000	0,082	0,116	0,062	0,623	0,029	11,9	3,55	0	0,12	0,0051	6,6	1,51	133,6	33,3	13,4
	TL-73-6	21,48	5,25	0,54	97,13	87,79	3,94	463,55	114,11	43,30	6,45	419,41	0,02	0,32	0,00	0,136	0,083	0,095	0,139	3,260	0,131	4,2	0,78	18,7	0,00	0,0425	12,6	3,51	168,1	25,5	13,8
	TL-73-7	44,49	5,79	0,92	49,24	302,07	6,03	614,51	96,62	40,92	3,4	341,30	0,39	14,77	0,00	0,000	0,088	0,104	0,065	0,747	0,070	0	0,36	268,3	0,01	0	12,4	1,46	144,8	101,9	146
Beaufor	TL-10-1	8,15	3,75	0,70	77,09	42,96	2,39	821,83	59,77	38,77	5,09	777,68	0,16	0,06	1,95	0,000	0,037	0,214	0,081	3,107	0,049	2,5	1,80	0	2,58	0	11,9	3,62	46,5	3,7	2,5
	TL-10-2	6,45	3,45	0,32	31,11	39,39	4,41	679,03	55,69	33,52	7,3	742,37	0,01	0,49	0,02	0,044	0,073	0,092	0,063	3,277	0,065	0	1,41	14,6	0,37	0	7,6	3,08	455,1	3,4	1,5
	TL-10-3	8,44	3,45	1,49	36,51	34,98	2,67	672,41	61,81	33,84	1,73	903,34	0,00	0,01	0,00	0,000	0,027	0,177	0,064	2,275	0,061	0	1,38	0	0,03	0	12,9	3,46	53	0	2,5
	TL-10-4	2,21	3,29	0,24	73,86	65,54	2,67	453,88	91,52	36,35	3,38	302,41	0,00	0,13	0,00	0,014	0,043	0,095	0,087	2,089	0,000	0	0,43	22,8	0,03	0,0204	9,2	1,52	52,6	6,6	3,9
	TL-10-5	4,52	3,60	0,83	36,68	57,22	3,70	545,06	73,18	34,01	4,92	390,54	0,02	0,18	0,00	0,000	0,041	0,222	0,094	2,258	0,068	8	0,92	23,8	0,09	0	7	1,58	98	14,8	4,9
	TL-10-6	3,46	4,16	2,84	23,87	58,58	3,04	614,68	87,79	35,05	4,41	920,32	0,01	0,36	0,01	0,000	0,034	0,182	0,059	1,969	0,065	0	2,04	10,2	0,05	0,0289	9,2	2,89	149,4	101,9	14,3
	TL-10-7	5,86	3,70	0,44	23,79	67,58	2,58	492,42	83,54	31,58	4,41	333,15	0,01	0,15	0,04	0,000	0,061	0,151	0,085	2,479	0,099	0	0,63	56	0,03	0,2887	18,7	2,51	134,1	339,6	356,6
	TL-10-8	5,14	3,92	0,51	50,09	48,90	3,41	708,07	70,64	38,04	3,4	743,72	0,01	0,65	0,03	0,000	0,083	0,031	0,064	2,292	0,053	0	0,98	4,9	0,06	0	9,7	2,97	108,7	11,9	0

1
2

Mine	Sample	Rare Earth element La	Ce	Pr	Nd	Sm	Eu	Gd	Tb	Dy	Ho
		ppm									
Goldex	TL-91-1	0,056	0,112	71,000	0,127	0,000	0,059	0,000	0,000	0,000	0,000
	TL-91-2	0,018	0,066	41,000	0,037	0,000	0,032	0,000	0,000	0,000	0,000
	TL-91-3	0,119	0,195	0,014	0,093	0,032	0,059	63,000	25,000	83,000	22,000
	TL-91-4	0,211	0,374	0,031	0,136	0,019	0,095	0,117	8,000	0,044	95,000
	TL-91-5	0,122	0,151	0,016	0,099	0,014	0,058	0,043	0,000	0,014	0,000
	TL-91-6	0,083	0,165	0,016	0,068	0,000	0,065	0,012	0,000	0,012	22,000
	TL-91-7	0,092	0,161	0,017	0,068	0,000	0,049	0,017	2,000	0,000	0,000
	TL-91-8	0,168	0,306	0,037	0,054	0,000	0,046	0,080	22,000	0,000	39,000
Lamaque											
Parallel	TL-88-1	5,264	14,942	1,817	7,132	1,308	0,229	0,662	0,127	0,543	0,059
	TL-88-2	0,071	0,166	61,000	0,027	0,000	0,042	0,000	2,000	0,000	49,000
	TL-88-3	0,126	0,175	0,018	0,068	0,024	0,054	0,000	1,000	0,000	58,000
	TL-88-4	0,054	0,131	95,000	0,054	0,000	0,043	0,048	54,000	0,010	61,000
	TL-88-5	0,093	0,100	0,026	0,200	0,093	0,044	0,000	0,000	0,029	83,000
	TL-88-6	4,924	13,075	1,698	7,132	1,596	0,226	1,817	0,268	1,783	0,365
	TL-88-7	0,109	0,338	0,025	0,078	0,011	0,050	0,056	65,000	0,048	0,012
	TL-88-8	0,116	0,166	0,013	0,075	0,000	0,102	0,043	0,000	42,000	22,000
Triangle	TL-87-1	0,408	1,172	0,141	0,985	0,250	0,189	0,472	0,105	0,815	0,172
	TL-87-2	0,049	0,306	0,028	0,340	0,149	0,153	0,255	0,037	0,282	0,112
	TL-87-3	0,073	0,172	0,025	0,116	0,027	0,139	0,061	0,015	0,151	0,037
	TL-87-4	0,075	0,214	0,036	0,206	0,105	0,121	0,296	0,082	0,642	0,231
	TL-87-5	0,099	0,465	0,112	0,730	0,662	0,248	0,951	0,216	1,834	0,336
	TL-87-6	2,615	6,792	0,781	3,888	0,815	0,172	0,781	0,134	0,883	0,190
	TL-87-7	1,036	2,666	0,391	1,783	0,883	0,443	1,392	0,246	1,698	0,301
	TL-87-8	0,093	0,110	0,019	0,066	0,056	0,148	0,015	37,000	0,054	37,000
	TL-85-1	0,141	0,212	0,025	0,121	0,041	0,112	0,148	0,032	0,199	0,075
	TL-85-2	0,063	0,163	0,012	0,126	0,000	0,116	0,010	0,000	53,000	0,000
	TL-85-3	0,093	0,239	0,046	0,122	0,061	0,099	0,036	88,000	0,058	0,027
	TL-85-4	1,240	3,175	0,448	2,224	0,730	0,318	0,832	0,160	1,189	0,418
	TL-85-5	0,146	0,207	0,033	0,117	0,044	0,104	0,105	0,030	0,299	0,112
	TL-85-6	0,231	0,425	0,095	0,380	0,129	0,187	0,183	0,049	0,348	0,116
	TL-85-7	0,058	0,134	0,018	0,063	0,000	0,112	0,000	73,000	0,043	0,015
	TL-85-8	0,764	2,360	0,377	2,123	0,832	0,299	0,883	0,144	1,070	0,219
Lac Herbin	TL-73-1	0,178	0,442	0,056	0,136	0,034	0,258	0,000	27,000	0,000	25,000
	TL-73-2	0,172	0,318	0,037	0,289	0,000	0,197	0,000	0,000	0,000	0,000
	TL-73-3	0,043	0,063	15,000	0,000	0,000	0,097	0,000	0,000	0,000	0,000
	TL-73-4	0,099	0,263	0,043	0,238	0,000	0,166	0,059	0,000	0,000	68,000
	TL-73-5	0,082	0,256	0,025	0,131	0,000	0,059	0,041	0,010	0,053	56,000
	TL-73-6	0,134	0,185	78,000	0,022	0,024	0,116	0,000	0,000	0,014	0,000
	TL-73-7	0,022	0,100	95,000	0,070	0,000	0,095	0,024	0,020	0,107	0,031
Beaufor	TL-10-1	0,070	0,126	0,023	0,046	0,000	0,105	8,000	0,000	39,000	46,000
	TL-10-2	0,110	0,183	0,016	0,076	0,000	0,136	41,000	0,000	0,000	0,000
	TL-10-3	0,097	0,206	0,022	0,066	0,000	0,160	0,000	0,000	0,000	0,000
	TL-10-4	0,017	0,025	0,000	0,000	0,000	0,027	0,000	0,000	0,000	0,000
	TL-10-5	0,025	0,048	0,000	0,000	0,000	0,044	0,000	0,000	0,000	12,000
	TL-10-6	0,073	0,246	0,030	0,168	0,000	0,121	0,000	0,000	0,000	37,000
	TL-10-7	0,041	0,075	0,000	0,000	0,000	0,013	0,063	0,000	0,000	73,000
	TL-10-8	0,088	0,148	0,022	0,070	0,000	0,121	0,000	0,000	0,000	0,000